

*Annual Review of Physical Chemistry*

# High-Field Dynamic Nuclear Polarization

Björn Corzilius

Institute of Chemistry and Department of Life, Light and Matter, University of Rostock,  
18059 Rostock, Germany; email: [bjoern.corzilius@uni-rostock.de](mailto:bjoern.corzilius@uni-rostock.de)

Annu. Rev. Phys. Chem. 2020. 71:143–70

First published as a Review in Advance on  
February 19, 2020

The *Annual Review of Physical Chemistry* is online at  
[physchem.annualreviews.org](http://physchem.annualreviews.org)

<https://doi.org/10.1146/annurev-physchem-071119-040222>

Copyright © 2020 by Annual Reviews.  
All rights reserved

## Keywords

dynamic nuclear polarization, DNP, nuclear magnetic resonance, NMR, electron paramagnetic resonance, EPR, polarizing agents, sensitivity enhancement, high magnetic field

## Abstract

Dynamic nuclear polarization (DNP) is one of the most prominent methods of sensitivity enhancement in nuclear magnetic resonance (NMR). Even though solid-state DNP under magic-angle spinning (MAS) has left the proof-of-concept phase and has become an important tool for structural investigations of biomolecules as well as materials, it is still far from mainstream applicability because of the potentially overwhelming combination of unique instrumentation, complex sample preparation, and a multitude of different mechanisms and methods available. In this review, I introduce the diverse field and history of DNP, combining aspects of NMR and electron paramagnetic resonance. I then explain the general concepts and detailed mechanisms relevant at high magnetic field, including solution-state methods based on Overhauser DNP but with a greater focus on the more established MAS DNP methods. Finally, I review practical considerations and fields of application and discuss future developments.

ANNUAL  
REVIEWS **CONNECT**

[www.annualreviews.org](http://www.annualreviews.org)

- Download figures
- Navigate cited references
- Keyword search
- Explore related articles
- Share via email or social media

---

**Cross-polarization (CP):** polarization transfer between (nondegenerate) spins by application of (electromagnetic) spin-lock fields, resulting in effectively equal rotating-frame frequencies

---

## 1. INTRODUCTION

### 1.1. NMR, Atomic Information, and the Sensitivity Problem

After its discovery by Bloch (1) and Purcell et al. (2) in 1946, nuclear magnetic resonance (NMR) quickly became one of the most widely applied analytical tools for the characterization of chemical compounds, biomolecular assemblies, or materials on an atomic scale. The rather small magnitude of the nuclear spin angular momentum, and thus the weak nuclear Zeeman interaction, leads to a unique advantage of NMR over other spectroscopic techniques: An extremely small natural line width on the order of  $\Delta\omega/\omega \approx 10^{-9}$  and long lifetimes of the excited states yield detailed information about minute variations in local magnetic field due to local electron density distribution (i.e., chemical shielding) or other spins (i.e., spin–spin couplings). These interactions are generally anisotropic but are averaged to their isotropic magnitude in solution under the assumption of fast and isotropic tumbling of the analyte molecule. In the solid state, however, anisotropic line broadening occurs, which drastically reduces sensitivity and may cause severe overlap of individual resonances. Furthermore, strong dipole–dipole interactions often dominate over chemical shifts, particularly when  $^1\text{H}$  is involved. In modern solid-state NMR, this situation is alleviated by direct detection of heteronuclei, such as  $^{13}\text{C}$ ,  $^{15}\text{N}$ , or  $^{31}\text{P}$ , while sensitivity can be enhanced by cross-polarization (CP) transfer from  $^1\text{H}$  (3, 4). In principle, anisotropic interactions such as chemical-shift anisotropy (CSA) and dipole–dipole couplings can be averaged solely by magic-angle spinning (MAS) (5–7). However, the interactions are very often only partially averaged because of the finite MAS frequency, and heteronuclear spin decoupling via radio-frequency (RF) irradiation of  $^1\text{H}$  is applied during detection of the free induction decay (FID) to achieve higher resolution and sensitivity (8, 9). Recently, advances in very fast MAS with frequencies of 110 kHz and higher have shifted the focus to  $^1\text{H}$  detection, albeit only in minute sample volumes (10). However, because of chemical-shift distributions as well as magnetic susceptibility anisotropy, the intrinsic line width in solids may, rarely, approach the extreme narrowing limit in liquids (11, 12). As a result, the sensitivity of solid-state NMR is significantly reduced with respect to high-resolution NMR in liquids.

Furthermore, the sensitivity of NMR in general is intrinsically low due to the flip side of the small Zeeman energy splitting: The magnetic spin excited state (e.g.,  $|\beta\rangle$  for  $^1\text{H}$ ) is almost as equally populated as the ground state ( $|\alpha\rangle$  for  $^1\text{H}$ ) due to stochastic excitation by thermal energy. Under typical conditions, a Zeeman polarization (see the sidebar titled Magnetization, Polarization, and Population Difference) of only  $\sim 100$  ppm exists in thermal equilibrium, meaning that only this fraction of nuclear spins contributes to the measurable net resonance absorption signal. Therefore, NMR typically requires the averaging of several FIDs in order to improve the acquired signal-to-noise ratio. As this ratio increases only with the square root of the number of transient signals averaged, a tremendous factor of  $10^8$  would be saved in measurement if the nuclear spin could be prepared in the pure ground state.

### 1.2. Electron Spin to the Rescue

Even though the preparation of a nearly pure nuclear spin ground state is unfeasible under most practical conditions, increasing polarization by any significant amount may dramatically improve NMR sensitivity. Here, we turn to the electron spin: Its spin angular momentum is several orders of magnitude larger than that of any nucleus. Compared with the proton—which carries the largest nuclear spin moment of any stable isotope—it is  $\sim 660$ -fold larger; consequently, its polarization is larger by practically the same factor (13).

However, this larger magnetic moment comes with several challenges. The large Zeeman interaction has enabled electron paramagnetic resonance (EPR) to be applied mainly at low to medium magnetic fields, typically between 0.3 and 3.4 T. This is a consequence of the ready

## MAGNETIZATION, POLARIZATION, AND POPULATION DIFFERENCE

Polarization plays a central role in DNP; however, its definition is often ambiguous. For example, the macroscopic magnetic properties of a spin ensemble (e.g., its magnetization) are defined by the expectation value of the  $z$ -projection operator,  $\langle \hat{s}_z \rangle = \text{Tr}(\hat{s}_z \cdot \rho) = \sum_i m_s(i) p_i$ , where  $\rho$  is the density matrix and the populations of eigenstates  $i$  are described by its diagonal elements ( $p_i = \rho_{ii}$ ). This expectation value does not yield a complete and unique microscopic description for systems with more than two states. Therefore, the distribution of population states  $p_i$  must be directly evaluated because they yield the probability with which each eigenstate is occupied in the ensemble. From these, the absolute population difference between two spin states  $i$  and  $j$  can be defined as  $\Delta p_{ij} = p_i - p_j$ , together with the respective relative population difference, defined as  $P_{ij} = (p_i - p_j)/(p_i + p_j)$ .

For any two-state system,  $\Delta p_{ij}$  and  $P_{ij}$  are equal and proportional to  $\langle \hat{s}_z \rangle$ ; therefore, most descriptions make little differentiation between them. For coupled-spin or high-spin systems, however, these values differ considerably in both value and relevance for DNP.  $P_{ij}$  describes the relative ratio at which opposing spin transitions occur between this pair of states and determines the maximum theoretical DNP enhancement factor.  $\Delta p_{ij}$  describes the absolute net transition rate and thus may limit the experimental DNP enhancement.

availability of microwave ( $\mu\text{w}$ ) components in radar or superhigh-frequency communication technology. Higher-frequency sources are rarely available because of a combination of diminished demand (e.g., due to atmospheric absorption) and technological challenges limiting the available  $\mu\text{w}$  power. This lack of availability has contributed to the existence of the so-called terahertz gap (14). From a magnetic resonance viewpoint, this problem is exacerbated by the large magnitude of anisotropies and spin–spin interactions encountered for electrons, ranging from several megahertz up to tens or hundreds of gigahertz. The resulting spectral breadth requires the superconducting magnet to have wide-range sweepability due to frequency-bandwidth limitations.

### 1.3. DNP: A Marriage Between EPR and NMR

Shortly after the inception of EPR and NMR, Overhauser (15) had a groundbreaking idea: By keeping the electron spins in solid metal in saturation, hyperfine-coupled nuclei would adopt the thermal spin polarization of the electrons, which would thus enhance their NMR signal by  $\sim 1,000$ -fold. Initially, this hypothesis faced severe criticism: Reaching a state of saturation corresponds to approaching infinite spin temperature, but hyperpolarization requires effective cooling of the spin bath (16). Despite this (at first glance) nonintuitive situation, Carver & Slichter (17) pursued this idea and finally succeeded in directly measuring the enhanced  $^7\text{Li}$  NMR signal. This was the very first DNP experiment, and it paved the way for a multitude of different techniques and theories, stimulated both by creative thinking and, most often, by unexpected experimental observations.

Over the course of six decades, many flavors and applications of DNP have emerged. It is not possible to cover every aspect of this exciting method in a single article; therefore, this review is limited to  $\mu\text{w}$ -driven DNP, with a focus on experiments where NMR spectroscopy is in situ enhanced by DNP. I refer the reader to several excellent reviews for more in-depth study, particularly for applications of DNP or other hyperpolarization methods not covered here in detail (18–30).

### 1.4. Bringing DNP to High Magnetic Field

DNP was limited to low-field applications for a rather long time. The first applications of MAS to polymers and other materials, developed by the Wind (31, 32) and Schaefer (33) research groups

---

#### Saturation:

depletion of transition polarization and thus net absorption by strong irradiation with a resonant electromagnetic field

#### Hyperpolarization:

increase in the magnitude of polarization of a specific transition above its thermal-equilibrium value

---

---

**Continuous wave**

**(cw):** term used in relation to continuously applied electromagnetic fields without changes in amplitude, frequency, or phase

**Polarizing agent**

**(PA):** paramagnetic species added to the DNP sample in the form of stable radicals or paramagnetic metal ions

**Hyperfine interaction (HFI):**

magnetic spin–spin coupling between an electron and a nuclear spin, mediated by Fermi contact or dipole–dipole interaction

**DNP enhancement factor:**

ratio between NMR signal intensity with and without  $\mu\text{w}$  irradiation, not accounting for paramagnetic and depolarization effects

**Cross relaxation**

**(CR):** mechanism involving two-spin spin flips, triggered by fluctuations in mutual spin–spin coupling (scalar or dipolar)

**Spin diffusion (SD):**

exchange of polarization between (near-)degenerate spins based on homonuclear flip-flop transitions; typically driven by dipole–dipole coupling in solids

---

in the 1980s and early 1990s, were conducted only up to 1.4 T. Shortly thereafter, the field was revolutionized with the development of high-power/high-frequency cyclotron maser sources (i.e., gyrotrons) for continuous-wave (cw) DNP application by a collaboration between the Griffin and Temkin groups at the Francis Bitter Magnet Laboratory and the Plasma Science and Fusion Center, respectively, at the Massachusetts Institute of Technology (34). This class of  $\mu\text{w}$  sources—initially developed for pulsed plasma heating in tokamak fusion reactors—has opened the field to biomolecular and materials applications, initially between 5 and 9.4 T and recently to contemporary ultrahigh NMR fields up to 21.1 T (900 MHz  $^1\text{H}$  frequency) (13, 30, 35).

Because DNP requires EPR and NMR excitation at the same time, it not only increases the complexity of instruments and experiments but also requires a combined effort from the respective communities. Such effort has effectively brought the fields of EPR and NMR much closer together, after they had drifted apart over several decades. Furthermore, it has drawn significant attention from the radical chemistry community via the development of novel polarizing agents (PAs) (36), as well as from the field of high-frequency engineering for  $\mu\text{w}$  components (37), making DNP a truly interdisciplinary technique.

## 2. DNP: CONCEPTS AND MECHANISMS

From a basic textbook perspective, pure EPR or NMR transitions are distinguished by selection rules for allowed single-quantum (SQ) transitions (i.e.,  $\Delta m_S = \pm 1$  and  $\Delta m_I = 0$  for EPR or  $\Delta m_S = 0$  and  $\Delta m_I = \pm 1$  for NMR, where  $S$  and  $I$  refer to the electron and nuclear spin quantum numbers, and  $m_S$  and  $m_I$  are the respective magnetic spin quantum numbers, as is depicted in **Figure 1a** for an  $S = 1/2$ ,  $I = 1/2$  system). However, DNP relies on the mutual spin flips of one electron spin of a PA and a nuclear spin (in the simplest case). Such multispin transitions are mediated by the hyperfine interaction (HFI), resulting in the preferential enrichment of one nuclear magnetic spin state over the other. Thus, it is theoretically possible to quantitatively transfer the electron polarization to a nuclear spin. In practice, however, one obtains the effective DNP enhancement factor  $\epsilon$ , which is typically smaller than the theoretical maximum defined by  $\epsilon_{\text{max}} = \gamma_S/\gamma_I$ , where  $\gamma_S$  and  $\gamma_I$  are the gyromagnetic ratios of the electron and nuclear spin, respectively.

The  $\mu\text{w}$  irradiation either drives the mutual spin flips coherently or saturates the electron SQ transition, which allows for incoherent electron–nuclear ( $e$ – $n$ ) cross relaxation (CR) (**Figure 1b**). At the same time, nuclear longitudinal magnetization strives to return to thermal equilibrium via spin–lattice relaxation, which limits the DNP efficiency, or it may be exchanged between nuclei of the same type via spin diffusion (SD).

This interplay of different interactions in a multispin system harbors a multitude of potential transfer pathways between the PA's electron spin and the nuclear spins to be detected (**Figure 2a**). These pathways may occur in parallel but can be selectively addressed through the choice of NMR pulse sequence (**Figure 2b**). An important point is that SD can transport the enhanced polarization far from the paramagnetic center, allowing the detection of nuclear spins with insignificant HFI contribution and avoiding deleterious effects such as paramagnetic shifts or broadening (**Figure 1c** shows an example featuring RNA). However, before discussing these so-called macroscopic effects leading to tremendous signal enhancement in such a scientific sample (see Section 3.1), I describe the microscopic DNP mechanisms in more detail.

### 2.1. Mechanisms Based on Continuous Microwave Irradiation

At high magnetic field, the Zeeman effect is typically the dominant interaction for any spin involved in DNP. However, in the pseudo-high-field approximation (see the sidebar titled

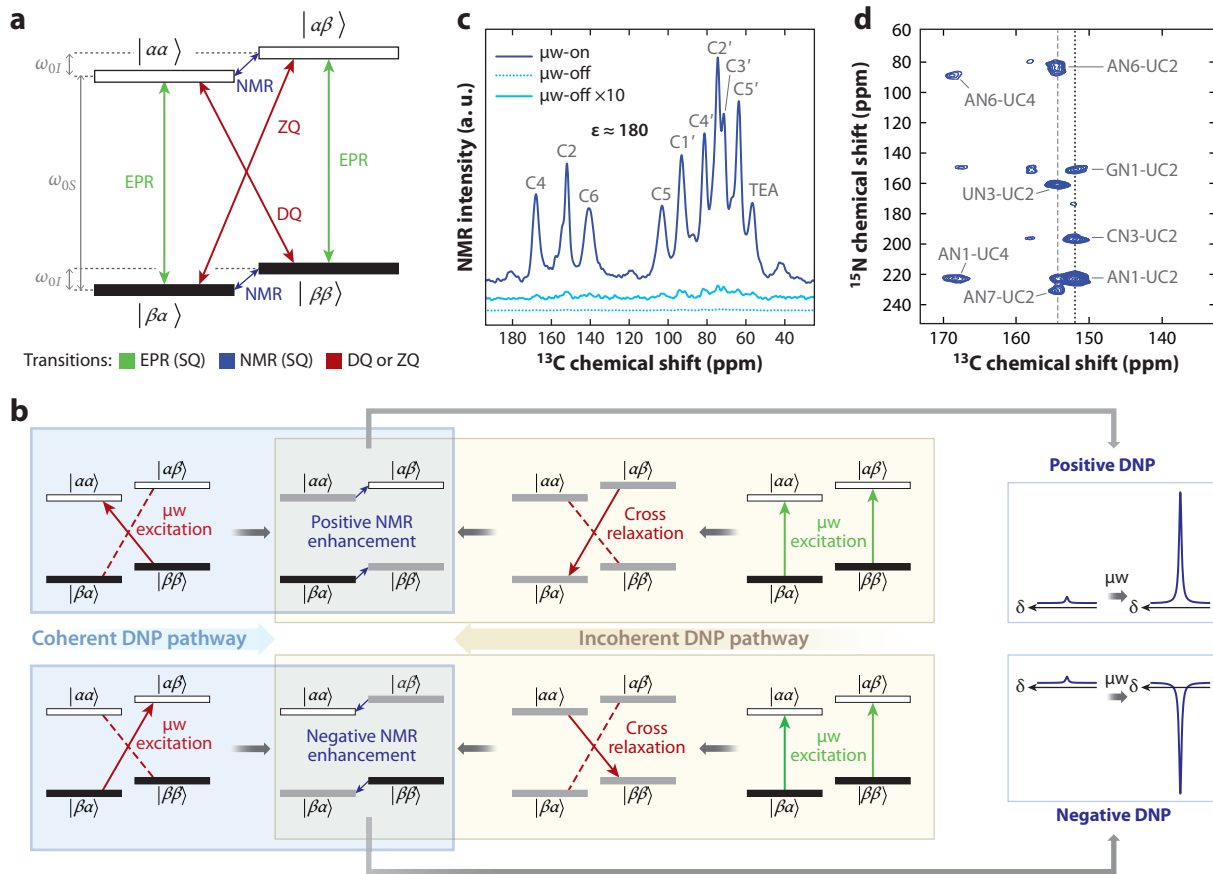


**Figure 1**

Schematic representation of the DNP principle. (a) Four-level system of an  $S = 1/2, I = 1/2$   $e-n$  two-spin system dominated by electron ( $\omega_{0,S}$ ) and nuclear ( $\omega_{0,I}$ ) Zeeman frequencies. All six possible transitions are represented by colored arrows; state populations (boxes) are coded by filling (black, strongly populated; white, weakly populated). (b) Coherent and incoherent pathways demonstrating general principles for creating positive or negative DNP. Each pathway starts from a system in thermal equilibrium at the far left or right. Gray states are medium populated as a result of saturation in a preceding step. DNP-enhanced MAS NMR (c)  $^{13}\text{C}$  CPMAS, (d)  $^{15}\text{N}$ - $^{13}\text{C}$  TEDOR on a 500- $\mu\text{M}$  frozen solution of a *trans*-acting full-length HHRz RNA using 5 mM AMUPol (89) as polarizing agent, yielding  $\sim 180$ -fold signal enhancement ( $\mu\text{w-on}/\mu\text{w-off}$  comparison) at 9.4 T (400 MHz). The  $\mu\text{w-off}$  signal is also shown with 10-fold multiplication for comparison. The HHRz was  $^{13}\text{C}_9$ -uridine labeled on the substrate strand and uniformly  $^{15}\text{N}$  labeled on the enzyme strand. The dotted vertical line marks correlation peaks arising from canonical base pairs; the dashed vertical line marks peaks from noncanonical (interstem) interactions. For further explanation and experimental details, see Reference 71. Abbreviations: CPMAS, cross-polarization magic-angle spinning; DNP, dynamic nuclear polarization; DQ, double-quantum transition; EPR, electron paramagnetic resonance; HHRz, hammerhead ribozyme; MAS, magic-angle spinning; NMR, nuclear magnetic resonance; SQ, single-quantum transition; TEA, triethanolamine; TEDOR, transferred-echo double resonance; ZQ, zero-quantum transition;  $\delta$ , chemical shift. Spectra adapted from Reference 71 with permission from Elsevier.

**Pseudo-High-Field Approximation and Pseudosecular Interactions: Basis for Solid-State DNP)** so-called forbidden transitions invoking changes of both magnetic spin quantum numbers may be rather inefficiently excited by coherent  $\mu\text{w}$  fields or incoherent local field fluctuations.  $\mu\text{w}$  fields are most often applied in a cw manner, addressing relatively slow transfer mechanisms such as the solid effect (SE) (38–41), cross effect (CE) (42–45), and Overhauser effect (OE) (15, 17). In these mechanisms, the fact that nuclear spin relaxation is even less efficient than DNP transfer

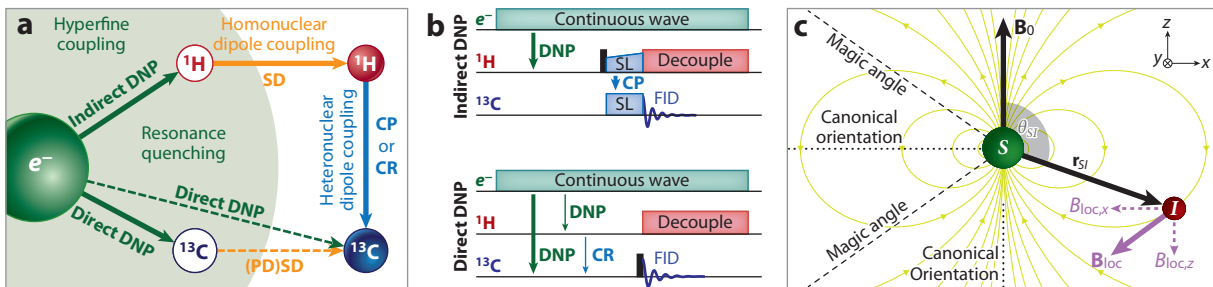


**Figure 2**

(a) Possible pathways for polarization transfer from an electron spin to NMR-detectable nuclear spins. Here, nuclear spins that are within a resonance-quenching sphere (light green) are undetectable by NMR due to paramagnetic effects and are shown as open circles. Dashed arrows show two potential but typically slow paths for direct DNP of detectable nuclei: either through direct DNP over long distances or via (PD)SD. (b) Basic pulse sequences for (top) indirect and (bottom) direct DNP. Thick arrows represent the primary pathways of polarization transfer; thin arrows describe a potential secondary pathway based on incoherent CR. (c) Dipole-dipole interaction between an electron spin ( $S$ ) and a nuclear spin ( $I$ ) in the  $z$ - $x$  plane. The nuclear spin senses the local field ( $B_{loc}$ ) generated by the electron spin, consisting of a longitudinal ( $B_{loc,z}$ ) and a transverse component ( $B_{loc,x}$ ), which depend on the  $e$ - $n$  distance vector's ( $r_{SI}$ ) magnitude and angle ( $\theta$ ) to the external magnetic field ( $B_0$ ). Whereas at the magic angle the longitudinal (i.e., secular) interaction vanishes, at the canonical orientations the transverse (i.e., pseudosecular) interaction is diminished. Abbreviations: CP, cross-polarization; CR, cross relaxation; DNP, dynamic nuclear polarization; FID, free induction decay; NMR, nuclear magnetic resonance; (PD)SD, (proton-driven) spin diffusion; SD, spin diffusion; SL, spin lock.

#### Solid effect (SE):

DNP mechanism within  $e$ - $n$  pairs, mediated by off-diagonal (pseudosecular) HFI; based on forbidden  $e$ - $n$  transitions

allows the accumulation of nuclear hyperpolarization with effective DNP buildup time constants ( $T_B$ ) on the order of the nuclear spin-lattice relaxation time constants ( $T_{1n}$ ). In contrast, pulsed DNP methods (discussed in Section 2.4, below) have attracted significant attention since they allow for much larger  $e$ - $n$  transfer rates. However, these methods presently suffer from several drawbacks, including increased instrumental and experimental complexity.

**2.1.1. OE.** The OE is the longest-known DNP mechanism and relies purely on incoherent  $e$ - $n$  transfer by CR. To achieve supportive conditions for OE DNP, the HFI must be time dependent in a stochastic manner, which is possible either in solid systems with mobile electrons such as metals or in solutions containing unpaired electrons. The OE was proposed by Overhauser (15)

### PSEUDO-HIGH-FIELD APPROXIMATION AND PSEUDOSECULAR INTERACTIONS: BASIS FOR SOLID-STATE DNP

Under the well-known high-field approximation, the electron and nuclear Zeeman interactions define the spin quantization frame along an external magnetic field, and all other interactions (e.g., spin-spin, quadrupolar) have a negligible impact. As such, only the secular term of the HFI (i.e.,  $A_{zz}\hat{S}_z\hat{I}_z$ ) commutes with the Zeeman operators ( $\hat{S}_z$  and  $\hat{I}_z$ ) and results in shifts of the eigenstates (i.e., hyperfine couplings) without causing any state mixing. All terms that do not commute with  $\hat{S}_z$  or  $\hat{I}_z$  may be dropped in a first-order approximation. These include all terms containing any of the orthogonal operators  $\hat{S}_x$ ,  $\hat{S}_y$ ,  $\hat{I}_x$ , and  $\hat{I}_y$ .

In the case of significant HFI, the high-field approximation is invalid for the nuclear spin but still reasonable for the electron due to the large difference in magnitude between the nuclear and electron Larmor frequencies. Therefore, the pseudo-high-field approximation is a good compromise in which the pseudosecular terms  $A_{zx}\hat{S}_z\hat{I}_x$  and  $A_{zy}\hat{S}_z\hat{I}_y$  are retained in addition to the secular HFI. This, however, results in mixing between the nuclear Zeeman states, which is the basis for SE and CE DNP.

## RELAXATION IN A SYSTEM OF TWO COUPLED SPINS: CROSS RELAXATION AND THE OVERHAUSER EFFECT IN A NUTSHELL

The magnetic moments of two spins subject to a strong external magnetic field are aligned by the Zeeman interaction. However, each spin creates its own local magnetic field, which may be sensed by the other spin either via dipole–dipole coupling or directly via Heisenberg exchange ( $e-e$ ), Fermi contact (FC) ( $e-n$ ), or  $J$  coupling ( $n-n$ ). If these local fields are undergoing stochastic fluctuation (e.g., by molecular motion), then SQ as well as zero-quantum (ZQ) and double-quantum (DQ) transitions may be induced by Fourier components matching the respective transition frequencies. These concepts, which give rise to autorelaxation (SQ) and CR (ZQ/DQ), were derived in a seminal paper by Solomon (48).

For OE DNP, a PA such as a nitroxide radical is saturated by  $\mu\omega$  excitation of the EPR SQ transition. Surrounding nuclear spins, which are under incoherently modulated HFI with the electron spin, may then experience stochastic NMR SQ, as well as  $e-n$  ZQ and DQ transitions; an imbalance in the latter causes nuclear hyperpolarization, while the system strives to reach equilibrium via relaxation. Note that  $e-n$  dipole–dipole coupling can potentially induce all transitions (i.e., SQ, ZQ, and DQ), whereas FC interaction may induce only ZQ transitions.

and shown by Carver & Slichter (17) to occur in lithium and subsequently in ammonia solutions of dissolved alkaline metals (46) or by use of radicals as PAs (47).

The OE can be quantitatively explained by Solomon's (48) theory of relaxation in a system of two spins (for a summary of the fundamental mechanism, see the sidebar titled Relaxation in a System of Two Coupled Spins: Cross Relaxation and the Overhauser Effect in a Nutshell).

The OE enhancement factor can be calculated by the steady-state solution of the Solomon equation in the following form:

$$\varepsilon - 1 = \underbrace{\frac{2W_1 + W_2 + W_0}{2W_1 + W_2 + W_0 + W_1^\circ}}_f \cdot \underbrace{\frac{W_2 - W_0}{2W_1 + W_2 + W_0}}_\xi \cdot \underbrace{\frac{P_S^\circ - P_S}{P_S^\circ}}_s \cdot \underbrace{\frac{\gamma_S}{\gamma_I}}_{\varepsilon_{\max}} = \frac{W_2 - W_0}{2W_1 + W_2 + W_0 + W_1^\circ} \cdot s \cdot \varepsilon_{\max}.$$

Here,  $W_i$  are the HFI-induced transition probabilities of the NMR SQ transition ( $i = 1$ ) as well as the  $e-n$  double-quantum (DQ;  $i = 2$ ) and zero-quantum (ZQ;  $i = 0$ ) transitions (**Figure 3a**). Additionally,  $W_1^\circ$  describes any inherent nuclear relaxation not caused by HFI. With knowledge of these rate constants (e.g., by analysis of the spectral density function of the local HFI field for  $W_i$  or by measurement of  $T_{1n}$  of a sample in the radical's absence for  $W_1^\circ$ ), the coupling factor  $\xi$  and the leakage factor  $f$  can be derived.  $\xi$  describes the ratio between  $e-n$  CR ( $W_2 - W_0$ ) and nuclear autorelaxation ( $2W_1 + W_2 + W_0$ ) (**Figure 3b**). In turn, the efficiency of all HFI-induced pathways with respect to the whole nuclear relaxation is given by  $f$ . The saturation factor  $s$  describes the efficiency of direct  $\mu\omega$  excitation of the EPR line, and  $\varepsilon_{\max}$  is the maximum enhancement factor given by the quotient of electron and nuclear gyromagnetic ratios. Both  $f$  and  $s$  may be assumed to approach unity for sufficiently large radical concentration and  $\mu\omega$  power (49); furthermore,  $s$  may be indirectly measured even without EPR detection capabilities by observation of the paramagnetic NMR lineshift (**Figure 3c**).

$\xi$  is a convolved function of the dynamics of the system, the magnetic field, and the strength and nature of HFI. In the simplest model, both Fermi contact (FC) and dipolar HFI are modulated by an isotropic tumbling of the nucleus around the electron spin, which is described by the mutual correlation time,  $\tau_c$ . The ratio of the mean-square FC and dipolar HFI is then described by the parameter  $\kappa$ , with  $\kappa = 1$  for a pure FC and  $\kappa = 0$  for a pure dipolar contribution to relaxation.

### Cross effect (CE):

DNP mechanism within  $e-e-n$  three-spin systems; efficiently driven by strong  $e-e$  coupling within biradicals

### Overhauser effect (OE):

DNP mechanism induced by fluctuations in HFI, based on  $e-n$  CR; mostly encountered in solution DNP

### DNP buildup:

gradual accumulation of nuclear hyperpolarization during DNP, typically obeying negative-exponential behavior similar to longitudinal relaxation

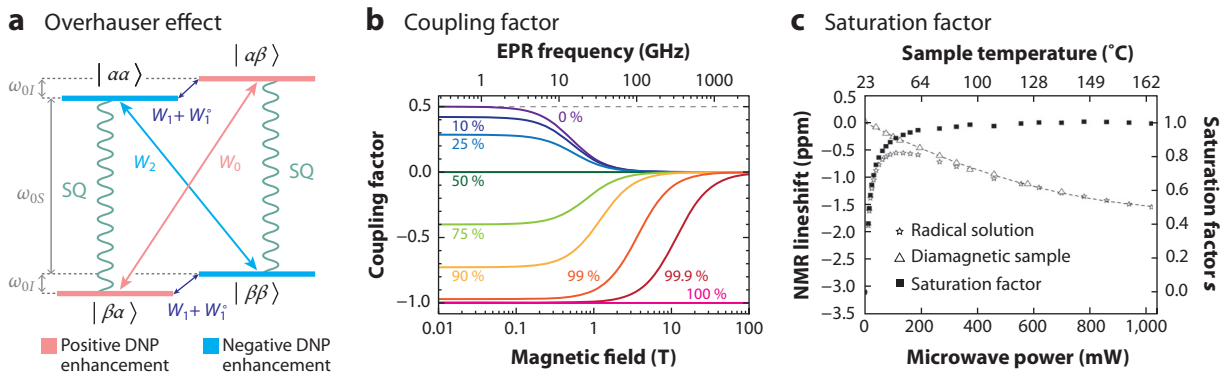


**Figure 3**

(a) Level diagram of an  $S = 1/2, I = 1/2$   $e-n$  two-spin system dominated by electron ( $\omega_{0,S}$ ) and nuclear ( $\omega_{0,I}$ ) Zeeman frequencies. During OE DNP, the EPR SQ transitions are saturated by  $\mu\text{W}$  irradiation; various relaxation pathways are represented by arrows. Transitions and thereby connected states leading to positive DNP enhancement are shown in light red, while those resulting in negative DNP enhancement are shown in light blue. (b) Coupling factor  $\xi$  as a function of the external magnetic field (or the EPR frequency for a  $g = 2$  electron spin) for a 20-ps correlation time for both scalar (FC) and dipolar HFI. The percentage relates to the ratio of the mean-square FC and dipolar HFI (factor  $\kappa$ ). (c) Dependence of sample temperature (*top axis*), NMR lineshift (*open symbols*: triangles, diamagnetic sample; stars, radical solution), and the saturation factor calculated therefrom (*filled squares*) on the  $\mu\text{W}$  power. Abbreviations: DNP, dynamic nuclear polarization; EPR, electron paramagnetic resonance; FC, Fermi contact; HFI, hyperfine interaction; NMR, nuclear magnetic resonance; OE, Overhauser effect; SQ, single-quantum transitions. Panel *c* adapted from Reference 49 with permission from the PCCP Owner Societies.

If the electron relaxation is very slow in relation to  $\tau_c$  (which is a good assumption for organic radicals), then  $\xi$  can be calculated as follows:

$$\xi = \frac{(1 - 2\kappa)j(\omega_{0,S})}{(1 - \kappa)[\frac{7}{5}j(\omega_{0,S}) + \frac{3}{5}j(\omega_{0,I})] + \kappa j(\omega_{0,S})}, \quad 2.$$

with the normalized spectral density function  $j(\omega) = 1/(1 + \omega^2\tau_c^2)$  (50). Therefore,  $\xi$  may take values ranging from  $-1$  (pure FC) to  $+0.5$  (purely dipolar HFI); a mixture of FC and dipolar HFI reduces the effective enhancement (50).

For molecular rotational and translational motion, the spectral density function quickly vanishes at high electron Zeeman frequencies. Thus—as long as a dipolar contribution to relaxation is present—nuclear autorelaxation dominates over CR, leading to diminishing  $\xi$  with increasing field (**Figure 3b**). Therefore, the OE is most effective and typically applied at lower magnetic field (e.g., 0.3 T, 9 GHz) (51). Efforts to develop robust and versatile DNP in liquids at room temperature and fields greater than 9 T are currently active in several laboratories worldwide, and the first important steps have been taken during the last decade (52–55).

Water is an excellent recipient for  $^1\text{H}$  OE DNP because it may closely approach the nitroxide moiety and form very short-lived contacts (25); therefore, it is typically much more effectively polarized by dipolar OE than are larger molecules, reaching enhancement factors of  $\sim 100$  at high field. However, a significant problem lies in the polarization transfer from water to an analyte of interest. Nevertheless,  $^1\text{H}$  within lipids may be directly hyperpolarized by OE DNP (56).

Direct OE DNP of  $^{13}\text{C}$  and  $^{31}\text{P}$ —where scalar (FC) relaxation dominates the OE mechanism—has shown very promising results at high magnetic field (53, 55, 57, 58). Enhancement factors of up to 1,000 have been obtained for  $^{13}\text{CCl}_4$  at 3.4 T (94 GHz) (59) and up to 70 for  $^{13}\text{CHCl}_3$  at 14.1 T (395 GHz) (55). In a groundbreaking demonstration, direct OE DNP of  $^{13}\text{C}$  enabled efficient hyperpolarization of metabolites at a field of 9.4 T without the need to transfer the polarization

### Fermi contact (FC) interaction:

scalar/isotropic interaction between nuclear and electron spins proportional to the electron's probability density at the nuclear position

from solvent and with uncompromised resolution of liquid-state NMR (54). This is an important step toward applicability of OE DNP.

Recently, OE was observed in a frozen solution of 1,3-*bis*(diphenylene)-2-phenylallyl (BDPA) radical at high magnetic field (60, 61). This finding is very promising, as excellent performance has been achieved in amorphous *ortho*-terphenyl at 18.8 T (527 GHz) with significant enhancement even at temperatures close to room temperature, while the efficiency of every other known DNP mechanism or PA vanishes under these conditions (62). The observation of efficient OE in insulating solids was rather unexpected, as the dynamics required for  $e$ - $n$  CR should be diminished at cryogenic temperatures. Fluctuations of spin density within BDPA's conjugated electronic system might be responsible for the required time dependence of FC interaction (61, 63); however, the contradictory presence of OE enhancement even at 1.2 K is still quite puzzling (64). Even though there is convincing evidence that the OE is indeed responsible for the aforementioned observations (61), considerably more research is required to completely explain the underlying mechanism. Interestingly, Han and colleagues (65) have shown that CE between a narrow-line radical and a radical with an extremely broad (i.e., undetectable) EPR line may pose as an OE lookalike.

**2.1.2. SE.** The SE is the first DNP mechanism known to occur in dielectric solids. It was independently discovered by three groups led by Jeffries (38, 39), Abragam (40), and Uebersfeld (41). Over the following decades, the SE has become a universally applied DNP mechanism because it may operate between a single electron spin and a dipolar-coupled nucleus. This property makes the SE very useful when other, potentially more efficient DNP mechanisms such as the CE become unviable—for example, when an intrinsic radical or metal ion is utilized as PA (66–71).

SE DNP relies on a local, dipolar HFI field transverse to the external magnetic field direction (which is defined as the laboratory frame  $z$  axis). Such a transverse field is present at the position of the nucleus if the  $e$ - $n$  connecting vector  $\mathbf{r}_{en}$  is not aligned along one of the canonical orientations with respect to the magnetic field  $\mathbf{B}_0$  [i.e., if  $\theta_{en} \equiv \angle(\mathbf{B}_0, \mathbf{r}_{en}) \neq n\pi/2$ , with  $n \in \mathbb{Z}$ ] (**Figure 2c**). While the longitudinal local field,  $B_{\text{loc},\parallel} \equiv B_{\text{loc},z} = -(\mu_0/4\pi) \cdot (g\mu_B/\hbar)|\mathbf{r}_{en}|^3 \cdot (3\cos^2\theta_{en} - 1)$ , provides the dipolar contribution to the spectral HFI splittings, the transverse field,  $B_{\text{loc},\perp} \equiv \sqrt{B_{\text{loc},x}^2 + B_{\text{loc},y}^2} = -(\mu_0/4\pi) \cdot (g\mu_B/\hbar)|\mathbf{r}_{en}|^3 \cdot 3 \sin\theta_{en} \cos\theta_{en}$ , induces partial mixing of nuclear spin states that allows weak excitation of  $e$ - $n$  ZQ and DQ coherences by  $\mu\text{w}$  excitation (**Figure 4a**). These transitions occur at the sum of or difference between the electron and nuclear Larmor frequencies (**Figure 4b**):

$$\omega_{\mu\text{w}}^{\text{ZQ/DQ}} \approx \omega_{0\text{S}} \mp \omega_{0\text{I}}. \quad 3.$$

The SE is rather ineffective at high magnetic field due to its relatively weak state mixing, which causes diminishing transition probabilities that scale with  $(\omega_{1\text{S}}B/2\omega_{0\text{I}})^2$ , where  $\omega_{1\text{S}}$  is the electron Rabi frequency and  $B \equiv \gamma_{\text{I}}B_{\text{loc},\perp}$  is the pseudosecular part of the HFI tensor components. The reason for this low efficiency is the rather small branching of nuclear spin quantization as a function of the electron magnetic spin state (**Figure 4c**). This is the result of competition between the relatively small dipolar HFI and the much larger nuclear Zeeman interaction (72–74).

The ZQ or DQ matching conditions (Equation 3) must be addressed selectively because they lead to opposite signs of nuclear hyperpolarization. This can be done if the overall EPR line width,  $\Delta_{\text{S}}$ , is sufficiently small compared with the nuclear Larmor frequency (i.e.,  $\Delta_{\text{S}} < \omega_{0\text{I}}$ ), such that the ZQ and DQ resonances are spectrally well resolved. If paramagnetic species with inhomogeneous line widths exceeding the nuclear Larmor frequency are used (i.e.,  $\Delta_{\text{S}} > \omega_{0\text{I}}$ ), then the SE efficiency is drastically reduced and the differential SE is observed (75). In this case,

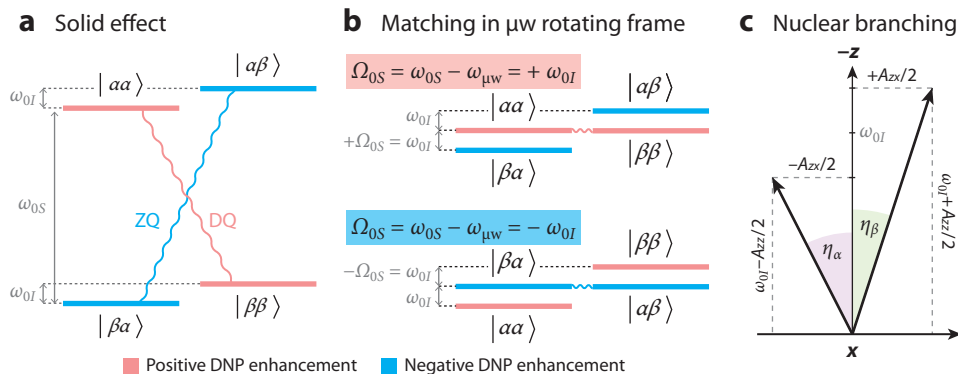


**Figure 4**

(a) Level diagram of an  $S = 1/2, I = 1/2$   $e$ - $n$  two-spin system dominated by electron ( $\omega_{0S}$ ) and nuclear ( $\omega_{0I}$ ) Zeeman frequencies for the SE in the laboratory frame. Transitions and thereby connected states leading to positive DNP enhancement are shown in light red, while those resulting in negative DNP enhancement are shown in light blue. (b) Level diagram in the  $\mu\text{w}$  rotating frame for the two possible SE matching conditions, resulting in degeneracy of states connected by either (*top*) DQ or (*bottom*) ZQ transitions. (c) Nuclear spin quantization branching responsible for mixing of nuclear spin states. Note that  $\omega_{0I}$  is typically  $\sim 2$  orders of magnitude larger than  $A_{zz}$  or  $A_{zx}$ . Abbreviations: DNP, dynamic nuclear polarization; DQ, double quantum; SE, solid effect; SQ, single quantum; ZQ, zero quantum;  $\mu\text{w}$ , microwave.

DNP enhancement may be recovered by application of more sophisticated techniques such as the integrated SE, either by rapid sweeping of the magnetic field through the whole EPR resonance (76) or by application of chirped  $\mu\text{w}$  pulses (77, 78), as is described in Section 2.3.1.

Despite its limited efficiency at high field, the SE is particularly versatile since it can be evoked by a wide variety of PAs, including radicals with a narrow EPR line such as trityl and BDPA (60, 74, 79) as well as paramagnetic transition-metal ions (80, 81). Nevertheless, it typically requires large incident  $\mu\text{w}$  power due to the small transition moment (13, 74).

**2.1.3. CE.** The CE is presently the most efficient cw DNP mechanism in rotating solids and occurs within three-spin systems consisting of two electron spins and a nucleus. It requires a pseudosecular HFI in combination with relatively large inhomogeneous broadening of the EPR line on the order of at least the nuclear Larmor frequency, as well as sufficiently strong electron-electron ( $e$ - $e$ ) interactions. The CE was first experimentally observed and theoretically described by Kessenikh and colleagues (42, 43, 82) as well as Hwang & Hill (44, 45) on the basis of intermolecular  $e$ - $e$  couplings in doped polymers under static NMR conditions. However, under the conditions investigated at very low temperatures (4.2 K and below), the EPR line is subject to strong spectral diffusion; as such, all electron spins participate for DNP, and the underlying mechanism may be better described by thermal mixing (TM) (83). Later, Atsarkin et al. (84) explained CE with distinct EPR lines caused by zero-field splitting of  $\text{Cr}^{3+}$  in ruby. The first description of CE with two EPR lines separated by the nuclear Larmor frequency—which is the basis for the modern treatment of this mechanism—was published by Wollan (85, 86) in 1976.

For CE to be active, the two coupled electron spins must differ in their effective Larmor frequencies by the nuclear Larmor frequency (**Figure 5a**):

$$\omega_{\Delta} = \omega_{0S_1} - \omega_{0S_2} \approx \pm\omega_{0I}. \quad 4.$$

**Zero-field splitting:** (typically quadrupolar) interaction of an electronic high-spin system with (internal or external) electric-field gradient

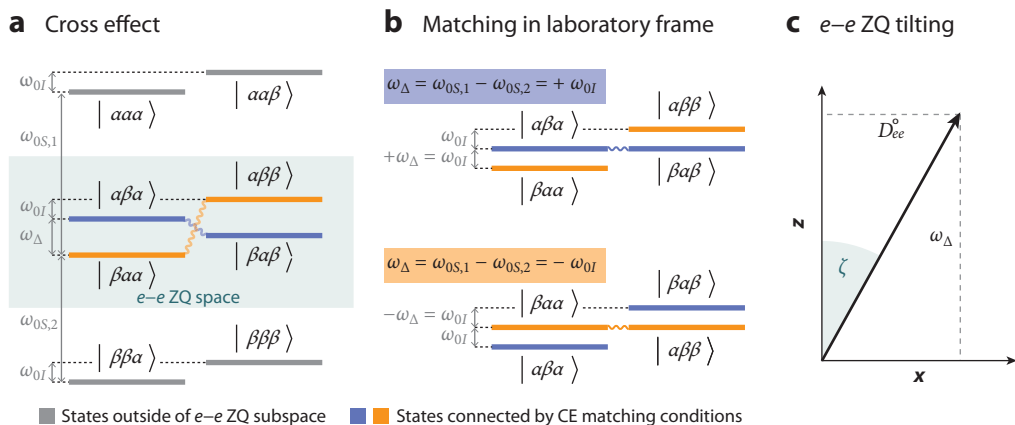


**Figure 5**

(a) Level diagram of an  $S_1 = S_2 = I = 1/2$   $e_1-e_2-n$  three-spin system dominated by electron ( $\omega_{0S}$ ) and nuclear ( $\omega_{0I}$ ) Zeeman frequencies for the CE in the laboratory frame. The two possible CE matching conditions connecting states within the  $e-e$  ZQ space (light green box) are shown in blue and orange. (b) Level diagram in the laboratory frame for the two CE matching conditions, resulting in degeneracy of states connected by three-spin-flip transitions. (c) Tilting of the effective field acting on the  $e-e$  pair in its ZQ subspace responsible for driving  $e-e$  flip-flop and  $e-e-n$  three-spin-flip transitions. Abbreviations: CE, cross effect; ZQ, zero quantum.

This EPR inequivalence is often realized by using tailored biradicals in which two radical moieties are tethered via a molecular linker (87) while preserving their individual doublet spin states; resonance frequency offsets are then achieved by anisotropic interactions. Prominent examples are the *bis*-nitroxides TOTAPOL (88), AMUPol (89), and bTbK (90). Recently, asymmetric biradicals comprising two chemically similar (e.g., AsymPol) or different (e.g., nitroxide and trityl/BDPA) radical species have shown significant advantages over their symmetric variants (35, 91, 92). In addition to organic biradicals, paramagnetic *bis*-complexes of  $Gd^{3+}$  can also evoke CE (93, 94).

By fulfilling the matching condition in Equation 4, energy may be efficiently exchanged between the electron and nuclear spins due to the relatively strong coupling of nearly degenerate states (**Figure 5b**). In order to reach net nuclear hyperpolarization, the two electrons must furthermore be differentially saturated (i.e., a spectral polarization gradient must be maintained), which is typically achieved by off-centered  $\mu w$  excitation of an inhomogeneously broadened EPR spectrum. The CE is particularly efficient under MAS, for which its theory has been elegantly described by a series of consecutive level anticrossings (LACs), as explained in Section 2.2 (95, 96). In static samples, the requirements for selective saturation of one electron spin and fulfillment of the CE matching condition (Equation 4) in a concerted manner often lead to reduced efficiency of this direct CE. This can be compensated for in the indirect CE by an electron polarization differential induced by spectral diffusion (97); its efficiency strongly increases with concentration of the PA. At very low temperature, the electron spin relaxation is diminished, and the collective response of all coupled electron spins gives rise to the TM DNP mechanism (98). This mechanism, not discussed in detail here, typically occurs for high radical concentrations at temperatures of 4 K or below, and it is utilized mainly in dissolution DNP (99).

The superior efficiency of the CE in comparison to the SE stems from the fact that—instead of the rather weak  $\mu w$  field—the much stronger  $e-e$  coupling is driving an  $e-e-n$  triple spin flip between two states within the significantly tilted  $e-e$  ZQ subspace (**Figure 5c**) (73, 100). Nevertheless, manipulating the nuclear spin state still requires pseudosecular HFI, similarly to the SE. As long as all spin-spin couplings are smaller than the nuclear Zeeman interaction, the resulting

#### Level anticrossing

**(LAC):** avoided crossing of states coupled by an off-diagonal Hamiltonian element during a time-dependent evolution

transition probability is proportional to  $(D_{ee}^\circ B/\omega_{0l})^2$ , where  $D_{ee}^\circ \equiv -(d_{ee} + 2J_{ee})$  is the effective  $e-e$  coupling, with  $d_{ee} = (\mu_0/4\pi) \cdot (g_1 g_2 \mu_B^2/\hbar) |\mathbf{r}_{ee}|^{-3} \cdot (3\cos^2\theta_{ee} - 1)$  and  $J_{ee}$  the Heisenberg exchange interaction. Therefore, the CE suffers from an equally detrimental dependence on the external magnetic field as the SE (101); however, it can be more easily compensated for by strategically increasing the  $e-e$  coupling in biradicals (91).

## 2.2. EPR Anisotropy and Level Crossings Under MAS

Under MAS, sample rotation causes a coherent and periodic modulation of all anisotropic interactions. For any interaction that is small compared with the frequency of rotation,  $\omega_r$ , the spin system behaves fully diabatically upon the modulation of eigenstates by MAS. Thus, the anisotropy is effectively averaged, leaving the isotropic interactions behind. This situation is often met for several NMR interactions, such as CSA of light nuclei or dipolar couplings between nuclear spins. If electron spins are involved, however, the anisotropic interactions are typically several orders of magnitude larger than  $\omega_r$ . This results in a significantly adiabatic behavior, such that the spin populations may evolve under the relatively slowly modulated eigenstates.

As a consequence, all solid-state DNP mechanisms must be reconsidered under the MAS rotation. To do so, it is convenient to describe all essential transitions leading to DNP in the framework of consecutive LACs occurring during each rotor period (95, 96). Hediger et al. (102) recently published an excellent review describing this situation and the resulting practicalities.

**2.2.1. SE.** For the SE, an  $e-n$  ZQ or DQ coherence must be directly induced (Equation 3). The resulting transition may be described by an LAC within the  $\mu w$  rotating frame (**Figure 4b**) (96). The adiabaticity is then determined by the rate with which this LAC is passed (given by the anisotropy and the MAS frequency) as well as by the coupling between the two states (given by the SE transition moment). In a simple model, the Landau-Zener formalism may be evoked to calculate the adiabaticity factor and the resulting probability that a transition will occur during the LAC (95). By consideration of the LACs occurring for all possible transitions (SE ZQ and DQ, EPR SQ) in the  $\mu w$  rotating frame, both (a) the competition between positive and negative DNP enhancement and (b) off-resonant saturation of the EPR transition can be understood and simulated (103).

**2.2.2. CE.** For the CE, the addition of a second electron spin leads to the further occurrence of both  $e_1-e_2-n$  three-spin CE LACs as well as  $e_1-e_2$  flip-flop LACs (95, 96). These LACs always appear in the  $e_1-e_2$  ZQ subspace in the laboratory frame without involvement of  $\mu w$  irradiation (**Figure 5b**). Thus, a  $\mu w$  LAC between two spin states connected by an EPR SQ transition may be temporally independent of the CE LAC, given that the polarization depletion of one electron spin imprinted during the former is memorized at the time of the latter. This is achieved if the electron longitudinal relaxation time constant,  $T_{1e}$ , is at least on the order of the rotational period,  $\tau_r = 2\pi/\omega_r$ . If one of the two electron spins is preferentially saturated during the  $\mu w$  LAC, a small fraction of the resulting difference in their polarization is then transferred to the nucleus during the weakly adiabatic CE LACs. Due to the very long  $T_{1n}$ , these small transfer steps may then accumulate nuclear hyperpolarization over many rotational periods, until a periodical steady-state condition is reached.

If two electron spins with similarly large anisotropic broadening of their EPR spectra are participating in the CE (as is the case for *bis*-nitroxide PAs), it is likely that at some point during the rotor period the two electrons will swap their order in frequency space and an opposite CE LAC will occur in which the sign in the CE matching condition (Equation 4) is inverted. Similarly to

the SE, the direction of polarization transfer is opposite for two such CE LACs; however, they must always be separated by a highly adiabatic  $e-e$  LAC (see Section 2.2.3) during which the polarizations of the two electrons are almost quantitatively exchanged. Therefore, all CE LACs may contribute to accumulating net enhancement on the nucleus.

CE effectively couples the nuclear polarization to the differential electron polarization independently of  $\mu\text{w}$  irradiation. As a result, CE-active PAs also act as superb longitudinal relaxation agents: Within an electron spin system that exchanges polarizations adiabatically, the MAS CE efficiently drives the HFI-coupled nuclear spins back to thermal equilibrium. This process results in the typically observed equality of DNP buildup ( $T_B$ ) and relaxation ( $T_{1n}$ ) time constants of CE-PA-doped samples (102). In contrast, in the case of SE,  $T_B$  is accelerated under  $\mu\text{w}$  irradiation with respect to  $T_{1n}$  (74, 79).

**2.2.3. Nuclear depolarization.** Despite the relatively high adiabaticity of  $e-e$  LACs, even small deviations from ideal behavior may accumulate and lead to a significant equilibration of the polarizations of the two electron spins if  $T_{1e} > \tau_r$ . Consequently, this process will reduce the polarization enhancement on the nucleus and also cause nuclear depolarization if no  $\mu\text{w}$  irradiation is applied, eventually leading to a reduced intensity of the  $\mu\text{w}$ -off signal (104, 105). The resulting exaggeration of the enhancement factor must be considered when assessing the actual sensitivity advantage gained by DNP; ideally, the sensitivity gain is compared with that of an identical sample but in the absence of PA (102). The detrimental effect of the lower electron polarization difference available for transfer to nuclei may be alleviated or even avoided by increasing the effective  $e-e$  coupling in the biradical (e.g., by exchange interaction) (92) or when using asymmetric biradicals of which one is a narrow-line radical with very small anisotropy, such as trityl or BDPA (35, 91, 106).

## 2.3. DNP with Incoherent Microwave Pulses

The ability to vary the frequency or amplitude of the  $\mu\text{w}$  field creates many possibilities for more efficient manipulations of the spin space in comparison to cw irradiation. Such manipulations have been demonstrated with low-power  $\mu\text{w}$  sources (107, 108). For MAS DNP, the higher required  $\mu\text{w}$  power necessitates specialized hardware such as frequency-agile gyrotrons (109–111), since the currently commercially available gyrotrons or extended interaction oscillators typically operate under cw conditions only (37).

**2.3.1. Frequency modulation and FS-ISE/S<sup>2</sup>E.** Similar to field modulation, simple frequency modulation of a continuous  $\mu\text{w}$  field can be used to increase the effective excitation bandwidth of inhomogeneously broadened EPR lines for DNP (107, 108, 112). Using chirped  $\mu\text{w}$  pulses instead of a continuous  $\mu\text{w}$  field may lead to further interesting effects if the chirp pulses' sweep width is sufficient to excite several transitions during a single pulse, as observed for the stretched solid effect (S<sup>2</sup>E) (77, 78). Here, consecutive excitation of the  $e-n$  ZQ or DQ (both of which lead to SE) and the SQ EPR transition (which saturates the electron spin and depletes the polarization available for transfer) cause a shift of the SE matching condition with respect to the pulse center frequency, depending on both the sweep width and direction.

If the pulse's sweep width is sufficient to cover both SE transitions (as well as the allowed EPR transition in between), an adiabatic inversion of the EPR polarization may occur that inverts the sign of one SE transition and thus leads to accumulation of polarization generated by both ZQ and DQ instead of mutual cancellation, where  $\Delta_S \gg \omega_{0I}$ . Therefore, this frequency-swept integrated SE (FS-ISE) is able to provide DNP enhancement from single paramagnetic sites with large inhomogeneous broadening of their EPR spectrum (77, 78).

---

**Depolarization:**  
reduction of nuclear spin polarization without  $\mu\text{w}$  irradiation under MAS by nonadiabatic  $e-e$  LACs within CE PAs

---

Experiment	cw DNP	NOVEL	DSSE	NRF-DNP	TOP-DNP
Pulse sequence					
Required HFI	OE: FC or dipolar (secular) SE/CE: dipolar (pseudosecular)	Dipolar (pseudosecular)	FC and/or dipolar (secular)	FC and/or dipolar (secular)	Dipolar (pseudosecular)
Nuclear spin orientation	Longitudinal (laboratory frame)	Longitudinal (laboratory frame)	Transverse (rotating frame)	Transverse (rotating frame)	Longitudinal (laboratory frame)
DNP transition moment	$\frac{\omega_{1S} A_{zx}}{2 \omega_{0I}}$ (SE) $\frac{D_{ee}^c A_{zx}}{\omega_{0I}}$ (CE)	$\frac{A_{zx}}{2}$ (field-independent)	$A_{zx}$ (field-independent)	$A_{zx}$ (field-independent)	Field-independent

**Figure 6**

Overview of different pulsed DNP experiments in comparison to cw DNP. The DNP transition moment is shown under ideal matching conditions for each mechanism. Abbreviations: CE, cross effect; cw, continuous wave; DNP, dynamic nuclear polarization; DSSE, dressed-state solid effect; FC, Fermi contact; FID, free induction decay; HFI, hyperfine interaction; NOVEL, nuclear orientation via electron spin locking; NRF, nuclear-rotating-frame; OE, Overhauser effect; RF, radio frequency; SE, solid effect; TOP, time-optimized.

**2.3.2. Electron decoupling.** If the  $\mu\text{w}$  source is able to switch the output frequency sufficiently rapidly, it is possible to partially decouple the nucleus from the electron spin during NMR detection in an SE experiment. To this end, the nuclear spins are first hyperpolarized by irradiation at an EPR offset corresponding to the nuclei's Larmor frequency (Equation 3). After the polarization period, the  $\mu\text{w}$  frequency is quickly switched for on-resonant EPR excitation, and the NMR spectrum is recorded by FID. Similar to high-power decoupling of  $^1\text{H}$  used in MAS NMR for the observation of low- $\gamma$  nuclei (8, 9), this process results in a narrowing of the observed NMR spectrum due to a partial averaging of HFI (113). The  $\mu\text{w}$  field strength generated inside an MAS stator (114) is currently not sufficient to completely decouple the HFI, either because it is stronger than the decoupling field or because the large offsets of spin packets in the inhomogeneously broadened EPR line prevent efficient excitation of all electron spins. However, the decoupling efficiency can be improved by using chirped  $\mu\text{w}$  pulses (115).

## 2.4. Pulsed DNP Utilizing Coherent Spin Rotations

Frequency-agile gyrotrons can be used for the experiments described in the above section, but they do not allow for coherent manipulation of the spin magnetization vector. For such experiments (Figure 6), custom-built integral EPR/NMR/DNP spectrometers are typically required, as they feature low-power phase-locked  $\mu\text{w}$  sources as well as static samples situated inside a  $\mu\text{w}$ -resonant cavity (116–118).

**2.4.1. NOVEL.** Pulsed DNP was described independently in similar experiments by the Hausser (119) and Wenckebach (120) groups in the late 1980s. In nuclear orientation via electron spin locking (NOVEL), the electron spin magnetization is spin-locked in the transverse plane after an initial flip pulse, and effective energy matching is achieved between the rotating frame of the electron and the laboratory frame of the nuclear spins. The condition is similar to the Hartmann-Hahn matching encountered in heteronuclear CP (3, 121); however, the Rabi frequency of the electrons is matched to the Larmor frequency of the nuclei ( $\omega_{1S} \approx \omega_{0I}$ ). Under this condition, the pseudosecular HFI can drive the  $e-n$  transition without attenuation by the nuclear Larmor frequency. Therefore, nuclear hyperpolarization is very quickly built up along the  $z$  axis of the directly coupled nucleus during the single spin lock. By fast repetition, enhanced polarization may be

further accumulated on the many bulk nuclei via SD if the electron spin magnetization is allowed to recover by spin-lattice relaxation (122, 123).

At high field, though, achieving the NOVEL matching condition is extremely challenging because it requires electron Rabi frequencies on the order of tens to hundreds of megahertz, well outside the technical capabilities of current instruments. Recently, the matching condition has been broadened and the efficiency improved by increasing the bandwidth during a ramped-amplitude spin lock (124). Furthermore, off-resonant NOVEL has been demonstrated, where the requirement of large Rabi frequencies may be partially compensated for by an offset between the  $\mu\text{w}$  frequency of the spin-locking field and the electron Larmor frequency (125).

**2.4.2. Nuclear-rotating-frame DNP and dressed-state SE.** Other pulsed DNP schemes include RF irradiation of the nuclear spins such as nuclear-rotating-frame (NRF)-DNP or dressed-state SE (DSSE) (126–128). In NRF-DNP, the nuclear magnetization is spin-locked in the transverse plane on resonance, while the electrons are irradiated with an offset frequency according to the effective nuclear field in the rotating frame:

$$\omega_{\mu\text{w}} = \omega_{0\text{S}} \pm \sqrt{\omega_{0\text{I}}^2 + \frac{A^2}{4}} \approx \omega_{0\text{S}} \pm \frac{A}{2},$$

where  $A \equiv A_{zz}$  is the secular part of the HFI. The DSSE may be most easily described by reversing the roles of the electron and the nucleus: The electron is spin-locked on resonance and thus resembles a dressed state, while the nucleus is subject to RF irradiation with an offset according to the effective field acting on the electron:

$$\omega_{\text{rf}} = \omega_{0\text{I}} \pm \sqrt{\omega_{0\text{S}}^2 + \frac{A^2}{4}} \approx \omega_{0\text{I}} \pm \omega_{1\text{S}}.$$

Note that while in NRF-DNP the RF field strength during the spin lock is typically much smaller than the HFI, the situation is the opposite in DSSE (i.e., the  $\mu\text{w}$  field strength dominates over the HFI), resulting in rather different effective matching conditions.

In both experiments, the electron polarization is transferred to fast-decaying nuclear transverse magnetization, and as such, it is rather difficult to accumulate or propagate it within the nuclear spin network. In fact, for DSSE, no effective nuclear hyperpolarization has yet been observed experimentally, but the depletion of electron spin magnetization upon transfer to the nuclei has revealed a characteristic profile reminiscent of its matching condition (128). NRF-DNP, in contrast, has shown significant experimental sensitivity gains, which are caused by the very fast DNP transfer, on the order of a few tens of microseconds, while the one-shot signal enhancement is close to unity (127). Therefore, such transverse-transfer methods are effective in observing nuclei that undergo fast relaxation (126). Therefore, in combination with techniques currently under development, such as electron decoupling (113), it may be possible to specifically hyperpolarize and observe nuclei in direct contact with the electron spin.

**2.4.3. Time-optimized DNP.** Tan et al. (129) have demonstrated a fundamentally new approach stimulated by MAS NMR recoupling experiments. In time-optimized DNP (TOP-DNP), a  $\mu\text{w}$  pulse train is applied to the electron spin during the DNP buildup period. The repeated pulses and delays induce a composite rotation of the spin space with an effective frequency  $\omega_{\text{eff}}$ , which depends on the Rabi frequency, length, EPR offset, and separation of the pulses. As a result, the DNP  $\mu\text{w}$  frequency profile consists of several intercalated and evenly spaced peaks, each

resulting in positive or negative DNP enhancement. In comparison to NOVEL, TOP-DNP requires only  $\sim 7\%$  of the  $\mu\text{w}$  power but necessitates fast switching of the  $\mu\text{w}$  field on the order of the nuclear Larmor period, which is related to subnanosecond pulse lengths for high magnetic fields. Therefore, so far TOP-DNP has been demonstrated only at fields of 1.2 T or lower (129).

### 3. FROM THE POLARIZING AGENT TO THE ANALYTE: APPLICATIONS OF MAS DNP

#### 3.1. Indirect Versus Direct DNP

The large electron spin polarization may be transferred to different nuclear species present in the sample. On the basis of the combination of DNP mechanism and PA utilized, this can be either selective (e.g., SE with narrow-line PA) or unselective (e.g., CE with wide-line PA), depending on the nuclear spin species fulfilling the respective matching conditions (13). Once built up on the directly HFI-coupled nuclei, the enhanced polarization may propagate through the homonuclear network by SD and may further be transferred to other nuclear species. This complex situation therefore allows for several different application scenarios.

**3.1.1. Indirect DNP via  $^1\text{H}$ .** In solids, the most commonly polarized nucleus is  $^1\text{H}$ , since it features a large magnetic moment and abundance in most samples. The strong homonuclear dipole-dipole interactions ensure an efficient transfer of enhanced polarization through the nuclear bulk by SD (**Figure 2a**). This enhanced bulk polarization can then be transferred to other (insensitive) nuclei by a Hartmann-Hahn CP step (**Figure 2b, top**). Subsequently, either the DNP-enhanced FID is directly observed or the transverse magnetization is further evolved in a more sophisticated (e.g., multiresonance or multidimensional) experiment (13).

The advantage of indirect DNP via  $^1\text{H}$  lies in its generally high sensitivity gain with short polarization/recycle delays. It also ensures a virtually uniform enhancement of all resonances with negligible paramagnetic broadening as long as the proton spins are strongly and homogeneously coupled (i.e., their mutual polarization exchange is faster than its buildup and/or relaxation).

**3.1.2. Direct DNP.** In a direct DNP experiment, polarization is usually detected or utilized on the nuclear species that has received its polarization directly from an electron spin without involving a heteronuclear transfer step (**Figure 2a**). Longitudinal magnetization created by cw DNP is then flipped into the transverse plane by a single  $90^\circ$  RF pulse and either detected via Bloch decay or further evolved, as needed (**Figure 2b, bottom**).

Direct DNP can thus be utilized if the sample is lacking any  $^1\text{H}$  spins (70). Alternatively, direct DNP may be applied if a more specific (i.e., nonuniform) transfer pathway is of interest, for example, within systems containing endogenous PAs or localized PA tags (67, 68, 71, 130).

Nuclei with a low gyromagnetic ratio and low spin concentration typically feature diminished SD, resulting in heterogeneous DNP behavior of individual nuclei depending on their spatial relationship with the electron spin. In this SD-limited case, paramagnetic broadening of DNP-enhanced resonances is often observed and is more pronounced for short polarization periods, where nuclei close to an electron spin contribute more strongly to the measured spectrum (68).

**3.1.3. Heteronuclear cross talk during DNP buildup.** The clear distinction between indirect and direct DNP by choice of NMR detection (i.e., CP or single-pulse excitation) is blurred if  $^1\text{H}$  and the low- $\gamma$  nuclear species of interest dynamically exchange polarization during the buildup of enhanced longitudinal magnetization. Such a situation occurs when active motions give rise to

heteronuclear dipolar relaxation (131). While this is typically the major mechanism for nuclear autorelaxation and thus limited DNP efficiency, hyperpolarization of  $^1\text{H}$  may also cause transfer to, for example,  $^{13}\text{C}$  via CR within dynamically active methyl groups or molecular ring systems [specific cross relaxation enhancement by active motions under DNP (SCREAM-DNP)]. This process results in the occurrence of two parallel transfer pathways (i.e., direct  $e^- \rightarrow ^{13}\text{C}$  and indirect  $e^- \rightarrow ^1\text{H} \rightarrow ^{13}\text{C}$ ), where the CR transfer causes buildup of an inverted (i.e., emissive)  $^{13}\text{C}$  NMR signal if  $^1\text{H}$  polarization is positively enhanced (132–134).

SCREAM-DNP has recently been demonstrated as an effective tool to selectively detect biomolecular complexes where methyl groups have been specifically introduced by the bound ligand (135) and to investigate the retinal-binding active site of proteorhodopsin during its photocycle (136). Furthermore, it may be utilized to indirectly investigate the molecular dynamics giving rise to dipolar relaxation under DNP conditions (137).

### 3.2. Samples Amenable to DNP

Because in most samples of interest no suitable endogenous PA is inherently present, special sample preparation is necessary for DNP. This introduces the PA typically in the form of a persistent radical dissolved in a glass-forming solvent mixture. Freezing of this solution is necessary to provide the rigid dipolar network required for solid-state DNP, and the sample often must be cooled significantly below room temperature with the use of cryogenic gases such as nitrogen or helium. In the resulting frozen solution, the spins are immobilized and their relaxation is slowed down.

**3.2.1. Vitrified solutions and biomolecular assemblies.** The PA-containing, glass-forming solution may be used either to codissolve the analyte, which is often done in the case of biomolecular samples, or to wet insoluble materials, as is explained below. In terms of alternatives to the solvent-wetting approach, several solvent-free preparation methods have been developed; these are not a topic of this article but are described in more detail elsewhere (13).

In the case of homogeneous solutions, the sample freezing and glass formation may introduce inhomogeneous broadening of NMR spectra, particularly for biomolecular samples (13, 138). For aqueous systems, a  $\text{D}_8$ -glycerol/ $\text{D}_2\text{O}$ / $\text{H}_2\text{O}$  mixture of 60/30/10 vol% (i.e., DNP juice) is most often used (139). If organic solvents are preferred, for example, for the wetting of water-sensitive materials or compounds, tetrachloroethane has proven to be the solvent of choice (140).

The efficient spreading of polarization by SD ensures, on the one hand, that a small concentration of PAs (e.g.,  $\sim 10$  mM) is able to hyperpolarize a large concentration of nuclei (e.g., typically  $\sim 10$  M for  $^1\text{H}$  in DNP juice). On the other hand, it enables the intermolecular, relayed transfer of polarization to the analyte through the solvent over large distances of several hundreds of nanometers up to several micrometers (141, 142), while preventing the deleterious paramagnetic effects that would arise from a close spatial relationship between the analyte and PA (143–145).

In most applications, a PA is used in concentrations of up to  $\sim 20$  mM. Smaller concentrations may be preferable to avoid accelerated transverse relaxation and signal loss in experiments utilizing coherent mixing for heteronuclear recoupling (146), or if the radical may interact with the analyte phase (147, 148). This solvent-doping method is applicable to a wide range of sample formulations in biomolecular research, including soluble proteins and nucleic acids, membrane proteins, viral capsids, and whole virus particles and plant tissue, among others (13, 149–151).

DNP is particularly powerful for the study of specific components of large biomolecular complexes or within complex mixtures. The large sensitivity gain has thus allowed for unique structural investigations of a signal peptide within the exit channel of the complete ribosome (152) and of a fibrillar protein at endogenous concentration within cellular milieus (153).

---

**Specific cross relaxation enhancement by active motions under DNP (SCREAM-DNP):** may occur during direct DNP due to heteronuclear CR; leads to additional enhancement by molecular motions

**DNP juice:** common cryoprotective solvent mixture used in biomolecular DNP; consists of  $\text{D}_8$ -glycerol,  $\text{D}_2\text{O}$ , and  $\text{H}_2\text{O}$  in a 6:3:1 volume ratio

---

**3.2.2. Insoluble phases.** Insoluble materials may be wetted with PA solutions, which is attractive for biomaterials such as bone and biosilica, for microcrystalline or porous solids in materials science such as catalysts and metal–organic frameworks, or for pharmaceutical formulations (13, 30, 154). The sensitivity gain by DNP is particularly interesting for these materials because isotope labeling is often impossible or extremely expensive. It has enabled investigations of, for example, the effective dispersion and disorder of active pharmaceutical ingredients in tablets (155) and of surface-bound active species by surface-enhanced NMR spectroscopy (DNP-SENS) (154, 156). In the context of the latter method, DNP has revolutionized MAS NMR, as such low-concentration species in natural isotope abundance are normally inaccessible due to insufficient sensitivity.

The tremendous increase in sensitivity of DNP has also proven highly useful for NMR crystallography because of the unique possibility of recording  $^{13}\text{C}$ – $^{13}\text{C}$  as well as  $^{15}\text{N}$ – $^{13}\text{C}$  correlation spectra in natural abundance, despite the very small effective occurrences of spin pairs of only 0.012% or 0.004%, respectively (157, 158). The full sets of assigned chemical shifts thus obtained then serve as constraints for quantum chemical calculations (158). These constraints may even be refined by the direct measurement of both intra- and intermolecular spin–spin distances of up to  $\sim 7 \text{ \AA}$  (159). In the homonuclear case, these distances are accessible only in natural abundance due to potential interference of dipolar truncation (160).

## 4. CONCLUSION AND OUTLOOK

DNP is an integral magnetic resonance method at the interface between NMR and EPR. During the last few decades, it has evolved from an intriguing oddity into a powerful tool to boost NMR sensitivity in order to enable experiments that would otherwise be completely infeasible due to prohibitive time requirements. DNP has continuously stimulated numerous novel concepts and theories, particularly regarding many-spin effects and complex interplay between electron and nuclear spins, which differ in their magnetic moments by approximately three orders of magnitude. These developments have supported the growth of a highly creative and interdisciplinary community, which will ensure that DNP brings great potential into the future.

However, DNP faces several challenges. Particularly for biomolecular applications, DNP-enhanced MAS NMR faces powerful competition from emerging methods both inside and outside magnetic resonance, such as  $^1\text{H}$  detection under very fast MAS (161) and cryo-electron microscopy (162). Undoubtedly, each method will find its own scope of application utilizing its unique strengths. In particular, DNP may exploit its potential to provide additional selectivity in NMR by specific signal enhancement only of targeted species in complex environments (135, 163, 164). This property might be very useful for in-cell applications or, for example, for characterization of structural changes in materials under practical conditions. Furthermore, the specific decoration of biomolecules or surfaces with PA tags may provide additional distance information (68, 71). On the one hand, inhomogeneous broadening often hampers clear spectral assignment, but on the other hand, it provides useful information about conformational flexibility or heterogeneity, which is difficult to assess with other methods (165, 166).

Clearly, the development of DNP from a methodological viewpoint is far from over. In the near future, we will witness stepwise improvements as well as fundamental breakthroughs. These might include completely novel PAs, DNP mechanisms, or instrumental designs. Numerous examples of such developments can be found throughout DNP's past and present. For example, symmetric biradicals were created in 2004 (87) and are now an indispensable part of MAS DNP (167), while asymmetric biradicals have only recently become state-of-the-art PAs for DNP at ultrahigh field (35, 91). The iterative optimization of PAs by using high-field EPR and theoretical predictions has just begun and promises great advances in the future (92, 168–171). DNP-SENS was

first demonstrated in 2010 (156) and is now one of the fastest-growing applications of DNP (30, 154, 172). Paramagnetic metal ions were introduced in 2011 (80) and are currently being utilized for the investigation of highly reactive battery electrode materials (69, 70). SCREAM-DNP was recently discovered as a spurious effect in direct polarization experiments (132, 133), but it has already been utilized to selectively detect bound biomolecular complexes with very high specificity (135). Future developments might involve pulsed DNP methods and the respective hardware requirements (173). Other instrumentation advances are aimed toward highly sensitive MAS DNP at very low temperature (174) and economical operation with a closed-loop helium MAS system (175), or toward the introduction of novel MAS designs that improve the reliability of MAS DNP operation, such as in spinning spheres (176).

Despite these exciting developments, it should not be forgotten that—even though DNP was conceived more than six decades ago—the commercialization of high-field DNP-enhanced MAS NMR and thus its broad availability occurred only during the last 10 years. During this relatively short time, numerous research institutes worldwide have acquired DNP capability, and the scientific impact in terms of publications and citations has been growing exponentially ever since. In the future, this methodological growth will undoubtedly lead to numerous novel breakthroughs. At the same time, DNP-enhanced MAS NMR will further develop as a standard analytical method supporting the existing toolbox, adding invaluable information during multitool characterization of biomolecular structure and materials (177–179).

## SUMMARY POINTS

1. DNP at high magnetic field is a truly interdisciplinary technique. Not only has it brought the EPR and NMR communities closer together, but also it has strengthened collaborations between the larger fields of magnetic resonance, theory, synthetic chemistry, and high-frequency electrical engineering.
2. MAS DNP is already established as a powerful and versatile technique for tackling extremely challenging problems in structural biology and materials research with atomic-scale resolution.
3. DNP in solution still poses several methodical challenges for large-scale applicability at high NMR fields, but exciting breakthroughs have recently been made.
4. Spectrometers for DNP-enhanced MAS NMR have been commercially available since as early as 2009, and many such instruments are in operation worldwide at fields up to 21 T (900 MHz  $^1\text{H}$ , 592 GHz  $e^-$ ).
5. PAs provide large electron spin polarization and can come in the form of either persistent radicals, such as (*bis*-)nitroxides or trityl, or paramagnetic metal ions.
6. The mechanisms by which DNP operates at the microscopic scale are complex. Important new insights, particularly for the theory of CE DNP under MAS, have recently been gained.
7. By better understanding the theory, improved PAs have been designed with greater efficiency at very high magnetic field and a reduced tendency for nuclear depolarization.
8. Control over polarization transfer pathways and/or sample constitution enables specific DNP enhancement of a targeted analyte, thus not only increasing NMR sensitivity but also introducing selectivity.

## FUTURE ISSUES

1. The additional hardware required for DNP demands greater investment, often exceeding the cost of the actual NMR spectrometer. It also has a relatively large laboratory-space footprint.
2. OE DNP in solution may be on the brink of more general applicability for the enhancement of high-resolution NMR sensitivity; however, the issues of  $\mu\text{w}$  absorption and excessive sample heating persist.
3. The required sample freezing below the glass transition temperature may yield information about structural flexibility but results in inhomogeneous broadening and compromises spectral resolution, particularly for biomolecular samples.
4. The high consumption of liquefied gases for cryogenic MAS results in significant operational costs, which may be drastically reduced by commercial development of a closed-cycle refrigeration/MAS system that would allow sample temperatures approaching that of liquid helium.
5. DNP at very low temperatures could provide very high sensitivity gains but would pose additional challenges for PA development (e.g., to prevent nuclear depolarization due to excessive electron spin saturation) and instrumentation.
6. Understanding and predicting the complex behavior of the large number of spins involved in the full DNP process require very expensive many-spin calculations and simulations. Several major breakthroughs have already been made in the de novo prediction of quantitative DNP parameters.
7. Despite recent progress, DNP efficiency still typically decreases with higher magnetic field and higher sample temperature, both of which are required for improving spectral resolution by avoiding homogeneous or inhomogeneous broadening.
8. MAS DNP is yet to be routinely combined with high-resolution  $^1\text{H}$  detection, which would provide tremendous sensitivity gains.

## DISCLOSURE STATEMENT

The author is not aware of any affiliations, memberships, funding, or financial holdings that might be perceived as affecting the objectivity of this review.

## ACKNOWLEDGMENTS

I thank Robert G. Griffin for an introduction to the field, for ongoing support, and for providing helpful comments on the manuscript. Further discussions with Kong Ooi Tan about pulsed DNP are also acknowledged. I thank Victoria Aladin, Thomas Prisner, and Vasyl Denysenkov for comments and proofreading.

## LITERATURE CITED

1. Bloch F. 1946. Nuclear induction. *Phys. Rev.* 70:460–74
2. Purcell EM, Torrey HC, Pound RV. 1946. Resonance absorption by nuclear magnetic moments in a solid. *Phys. Rev.* 69:37–38
3. Pines A, Gibby MG, Waugh JS. 1972. Proton-enhanced nuclear induction spectroscopy. A method for high resolution NMR of dilute spins in solids. *J. Chem. Phys.* 56:1776–77

4. Pines A, Gibby MG, Waugh JS. 1973. Proton-enhanced NMR of dilute spins in solids. *J. Chem. Phys.* 59:569–90
5. Andrew ER, Bradbury A, Eades RG. 1958. Nuclear magnetic resonance spectra from a crystal rotated at high speed. *Nature* 182:1659
6. Andrew ER, Bradbury A, Eades RG. 1959. Removal of dipolar broadening of nuclear magnetic resonance spectra of solids by specimen rotation. *Nature* 183:1802–3
7. Lowe JJ. 1959. Free induction decays of rotating solids. *Phys. Rev. Lett.* 2:285–87
8. Bloch F. 1958. Theory of line narrowing by double-frequency irradiation. *Phys. Rev.* 111:841–53
9. Sarles LR, Cotts RM. 1958. Double nuclear magnetic resonance and the dipole interaction in solids. *Phys. Rev.* 111:853–59
10. Vasa SK, Rovó P, Linsler R. 2018. Protons as versatile reporters in solid-state NMR spectroscopy. *Acc. Chem. Res.* 51:1386–95
11. Samoson A, Tuhern T, Gan Z. 2001. High-field high-speed MAS resolution enhancement in  $^1\text{H}$  NMR spectroscopy of solids. *Solid State Nucl. Magn. Reson.* 20:130–36
12. Sternberg U, Witter R, Kuprov I, Lamley JM, Oss A, et al. 2018.  $^1\text{H}$  line width dependence on MAS speed in solid state NMR—comparison of experiment and simulation. *J. Magn. Reson.* 291:32–39
13. Lilly Thankamony AS, Wittmann JJ, Kaushik M, Corzilius B. 2017. Dynamic nuclear polarization for sensitivity enhancement in modern solid-state NMR. *Prog. Nucl. Magn. Reson. Spectrosc.* 102/103:120–95
14. Lee M, Wanke MC. 2007. Searching for a solid-state terahertz technology. *Science* 316:64–65
15. Overhauser AW. 1953. Polarization of nuclei in metals. *Phys. Rev.* 92:411–15
16. Slichter CP. 2010. The discovery and demonstration of dynamic nuclear polarization—a personal and historical account. *Phys. Chem. Chem. Phys.* 12:5741–51
17. Carver TR, Slichter CP. 1953. Polarization of nuclear spins in metals. *Phys. Rev.* 92:212–13
18. Ardenkjaer-Larsen JH. 2016. On the present and future of dissolution DNP. *J. Magn. Reson.* 264:3–12
19. Bornet A, Jannin S. 2016. Optimizing dissolution dynamic nuclear polarization. *J. Magn. Reson.* 264:13–21
20. Jähnig F, Kwiatkowski G, Ernst M. 2016. Conceptual and instrumental progress in dissolution DNP. *J. Magn. Reson.* 264:22–29
21. Comment A. 2016. Dissolution DNP for in vivo preclinical studies. *J. Magn. Reson.* 264:39–48
22. van Bentum J, van Meerten B, Sharma M, Kentgens A. 2016. Perspectives on DNP-enhanced NMR spectroscopy in solutions. *J. Magn. Reson.* 264:59–67
23. Lingwood MD, Han S. 2011. Solution-state dynamic nuclear polarization. *Annu. Rep. NMR Spectrosc.* 73:83–126
24. Ravera E, Luchinat C, Parigi G. 2016. Basic facts and perspectives of Overhauser DNP NMR. *J. Magn. Reson.* 264:78–87
25. Prisner T, Denysenkov V, Sezer D. 2016. Liquid state DNP at high magnetic fields: instrumentation, experimental results and atomistic modelling by molecular dynamics simulations. *J. Magn. Reson.* 264:68–77
26. Ardenkjaer-Larsen J-H, Boebinger GS, Comment A, Duckett S, Edison AS, et al. 2015. Facing and overcoming sensitivity challenges in biomolecular NMR spectroscopy. *Angew. Chem. Int. Ed.* 54:9162–85
27. Duckett SB, Mewis RE. 2012. Application of parahydrogen induced polarization techniques in NMR spectroscopy and imaging. *Acc. Chem. Res.* 45:1247–57
28. Kovtunov KV, Pokochueva EV, Salnikov OG, Cousin SF, Kurzbach D, et al. 2018. Hyperpolarized NMR spectroscopy: d-DNP, PHIP, and SABRE techniques. *Chem. Asian J.* 13:1857–71
29. Zhang G, Hilty C. 2018. Applications of dissolution dynamic nuclear polarization in chemistry and biochemistry. *Magn. Reson. Chem.* 56:566–82
30. Rankin A, Trébose J, Pourpoint F, Amoureux J-P, Lafon O. 2019. Recent developments in MAS DNP-NMR of materials. *Solid State Nucl. Magn. Reson.* 101:116–43
31. Duijvestijn MJ, van der Lugt C, Smidt J, Wind RA, Zilm KW, Staplin DC. 1983.  $^{13}\text{C}$  NMR spectroscopy in diamonds using dynamic nuclear polarization. *Chem. Phys. Lett.* 102:25–28

---

13. Comprehensively reviews all aspects of DNP-enhanced MAS NMR, including biomolecular and materials science applications.

---

32. Wind RA, Duijvestijn MJ, van der Lugt C, Manenschijn A, Vriend J. 1985. Applications of dynamic nuclear polarization in  $^{13}\text{C}$  NMR in solids. *Prog. Nucl. Magn. Reson. Spectrosc.* 17:33–67
33. Afeworki M, Vega S, Schaefer J. 1992. Direct electron-to-carbon polarization transfer in homogeneously doped polycarbonates. *Macromolecules* 25:4100–5
34. Becerra LR, Gerfen GJ, Temkin RJ, Singel DJ, Griffin RG. 1993. Dynamic nuclear polarization with a cyclotron resonance maser at 5 T. *Phys. Rev. Lett.* 71:3561–64
35. Wissler D, Karthikeyan G, Lund A, Casano G, Karoui H, et al. 2018. BDPA-nitroxide biradicals tailored for efficient dynamic nuclear polarization enhanced solid-state NMR at magnetic fields up to 21.1 T. *J. Am. Chem. Soc.* 140:13340–49
36. Casano G, Karoui H, Ouari O. 2018. Polarizing agents: evolution and outlook in free radical development for DNP. *eMagRes* 7:195–208
37. Blank M, Felch KL. 2018. Millimeter-wave sources for DNP-NMR. *eMagRes* 7:155–66
38. Jeffries CD. 1957. Polarization of nuclei by resonance saturation in paramagnetic crystals. *Phys. Rev.* 106:164–65
39. Abraham M, Kedzie RW, Jeffries CD. 1957.  $\gamma$ -Ray anisotropy of  $\text{Co}^{60}$  nuclei polarized by paramagnetic resonance saturation. *Phys. Rev.* 106:165–66
40. Abragam A, Proctor WG. 1958. Une nouvelle méthode de polarisation dynamique des noyaux atomiques dans les solides. *C. R. Hebd. Séances Acad. Sci.* 246:2253–56
41. Erb E, Motchane JL, Uebersfeld J. 1958. Effet de polarisation nucléaire dans les liquides et les gaz adsorbés sur les charbons. *C. R. Hebd. Séances Acad. Sci.* 246:2121–23
42. Kessenikh AV, Lushchikov VI, Manenkov AA, Taran YV. 1963. Proton polarization in irradiated polyethylenes. *Sov. Phys. Solid State* 5:321–29
43. Kessenikh AV, Manenkov AA, Pyatnitskii GI. 1964. On explanation of experimental data on dynamic polarization of protons in irradiated polyethylenes. *Sov. Phys. Solid State* 6:641–43
44. Hwang CF, Hill DA. 1967. Phenomenological model for new effect in dynamic polarization. *Phys. Rev. Lett.* 19:1011–14
45. Hwang CF, Hill DA. 1967. New effect in dynamic polarization. *Phys. Rev. Lett.* 18:110–12
46. Carver TR, Slichter CP. 1956. Experimental verification of the Overhauser nuclear polarization effect. *Phys. Rev.* 102:975–80
47. Beljers HG, van der Kint L, van Wieringen JS. 1954. Overhauser effect in a free radical. *Phys. Rev.* 95:1683
48. Solomon I. 1955. Relaxation processes in a system of two spins. *Phys. Rev.* 99:559–65
49. Neugebauer P, Krummenacker JG, Denysenkov VP, Parigi G, Luchinat C, Prisner TF. 2013. Liquid state DNP of water at 9.2 T: an experimental access to saturation. *Phys. Chem. Phys.* 15:6049–56
50. Hausser KH, Stehlik D. 1968. Dynamic nuclear polarisation in liquids. *Adv. Magn. Reson.* 3:79–139
51. Kaminker I, Barnes R, Han SI. 2015. Overhauser dynamic nuclear polarization studies on local water dynamics. In *Electron Paramagnetic Resonance Investigations of Biological Systems by Using Spin Labels, Spin Probes, and Intrinsic Metal Ions*, ed. PZ Qin, K Warncke, pp. 457–83. San Diego: Academic
52. Denysenkov V, Prisner T. 2012. Liquid state dynamic nuclear polarization probe with Fabry-Pérot resonator at 9.2 T. *J. Magn. Reson.* 217:1–5
53. Yoon D, Dimitriadis AI, Soundararajan M, Caspers C, Genoud J, et al. 2018. High-field liquid-state dynamic nuclear polarization in microliter samples. *Anal. Chem.* 90:5620–26
54. **Orlando T, Dervişoğlu R, Levien M, Tkach I, Prisner TF, et al. 2019. Dynamic nuclear polarization of  $^{13}\text{C}$  nuclei in the liquid state over a 10 Tesla field range. *Angew. Chem. Int. Ed.* 58:1402–6**
55. Dubroca T, Wi S, van Tol J, Frydman L, Hill S. 2019. Large volume liquid state scalar Overhauser dynamic nuclear polarization at high magnetic field. *Phys. Chem. Chem. Phys.* 21:21200–4
56. Jakdetchai O, Denysenkov V, Becker-Baldus J, Dutagaci B, Prisner TF, Glaubitz C. 2014. Dynamic nuclear polarization-enhanced NMR on aligned lipid bilayers at ambient temperature. *J. Am. Chem. Soc.* 136:15533–36
57. Dubroca T, Smith AN, Pike KJ, Froud S, Wylde R, et al. 2018. A quasi-optical and corrugated waveguide microwave transmission system for simultaneous dynamic nuclear polarization NMR on two separate 14.1 T spectrometers. *J. Magn. Reson.* 289:35–44

---

54. Presents a groundbreaking development in OE DNP for solution NMR at high magnetic field.

---

58. Bennati M, Orlando T. 2019. Overhauser DNP in liquids on  $^{13}\text{C}$  nuclei. *eMagRes* 8:11–18
59. Liu GQ, Levien M, Karschin N, Parigi G, Luchinat C, Bennati M. 2017. One-thousand-fold enhancement of high field liquid nuclear magnetic resonance signals at room temperature. *Nat. Chem.* 9:676–80
60. Haze O, Corzilius B, Smith AA, Griffin RG, Swager TM. 2012. Water-soluble organic radicals as polarizing agents for high field dynamic nuclear polarization. *J. Am. Chem. Soc.* 134:14287–90
61. Can TV, Caporini MA, Mentink-Vigier F, Corzilius B, Walish JJ, et al. 2014. Overhauser effects in insulating solids. *J. Chem. Phys.* 141:064202
62. Lelli M, Chaudhari SR, Gajan D, Casano G, Rossini AJ, et al. 2015. Solid-state dynamic nuclear polarization at 9.4 and 18.8 T from 100 K to room temperature. *J. Am. Chem. Soc.* 137:14558–61
63. Pylaeva S, Ivanov KL, Baldus M, Sebastiani D, Elgabarty H. 2017. Molecular mechanism of Overhauser dynamic nuclear polarization in insulating solids. *J. Phys. Chem. Lett.* 8:2137–42
64. Ji X, Can TV, Mentink-Vigier F, Bornet A, Milani J, et al. 2018. Overhauser effects in non-conducting solids at 1.2 K. *J. Magn. Reson.* 286:138–42
65. Equbal A, Li Y, Leavesley A, Huang S, Rajca S, et al. 2018. Truncated cross effect dynamic nuclear polarization: an Overhauser effect doppelgänger. *J. Phys. Chem. Lett.* 9:2175–80
66. Maly T, Cui D, Griffin RG, Miller A-F. 2012.  $^1\text{H}$  dynamic nuclear polarization based on an endogenous radical. *J. Phys. Chem. B* 116:7055–65
67. Wenk P, Kaushik M, Richter D, Vogel M, Suess B, Corzilius B. 2015. Dynamic nuclear polarization of nucleic acid with endogenously bound manganese. *J. Biomol. NMR* 63:97–109
68. Kaushik M, Bahrenberg T, Can TV, Caporini MA, Silvers R, et al. 2016. Gd(III) and Mn(II) complexes for dynamic nuclear polarization: small molecular chelate polarizing agents and applications with site-directed spin labeling of proteins. *Phys. Chem. Chem. Phys.* 18:27205–18
69. Chakrabarty T, Goldin N, Feintuch A, Houben L, Leskes M. 2018. Paramagnetic metal-ion dopants as polarization agents for dynamic nuclear polarization NMR spectroscopy in inorganic solids. *Chem. Phys. Chem.* 19:2139–42
- 70. Wolf T, Kumar S, Singh H, Chakrabarty T, Aussenac F, et al. 2019. Endogenous dynamic nuclear polarization for natural abundance  $^{17}\text{O}$  and lithium NMR in the bulk of inorganic solids. *J. Am. Chem. Soc.* 141:451–62**
71. Daube D, Vogel M, Suess B, Corzilius B. 2019. Dynamic nuclear polarization on a hybridized hammerhead ribozyme: an explorative study of RNA folding and direct DNP with a paramagnetic metal ion cofactor. *Solid State Nucl. Magn. Reson.* 101:21–30
72. Hovav Y, Feintuch A, Vega S. 2010. Theoretical aspects of dynamic nuclear polarization in the solid state—the solid effect. *J. Magn. Reson.* 207:176–89
- 73. Hu KN, Debelouchina GT, Smith AA, Griffin RG. 2011. Quantum mechanical theory of dynamic nuclear polarization in solid dielectrics. *J. Chem. Phys.* 134:125105**
74. Corzilius B, Smith AA, Griffin RG. 2012. Solid effect in magic angle spinning dynamic nuclear polarization. *J. Chem. Phys.* 137:054201
75. Abraham M, McCausland MAH, Robinson FNH. 1959. Dynamic nuclear polarization. *Phys. Rev. Lett.* 2:449–51
76. Henstra A, Dirksen P, Wenckebach WT. 1988. Enhanced dynamic nuclear-polarization by the integrated solid effect. *Phys. Lett. A* 134:134–36
77. Can TV, Weber RT, Walish JJ, Swager TM, Griffin RG. 2017. Frequency-swept integrated solid effect. *Angew. Chem. Int. Ed.* 56:6744–48
78. Can TV, McKay JE, Weber RT, Yang C, Dubroca T, et al. 2018. Frequency-swept integrated and stretched solid effect dynamic nuclear polarization. *J. Phys. Chem. Lett.* 9:3187–92
79. Smith AA, Corzilius B, Barnes AB, Maly T, Griffin RG. 2012. Solid effect dynamic nuclear polarization and polarization pathways. *J. Chem. Phys.* 136:015101
80. Corzilius B, Smith AA, Barnes AB, Luchinat C, Bertini I, Griffin RG. 2011. High-field dynamic nuclear polarization with high-spin transition metal ions. *J. Am. Chem. Soc.* 133:5648–51
- 81. Corzilius B. 2018. Paramagnetic metal ions for dynamic nuclear polarization. *eMagRes* 7:179–94**
82. Kessenikh AV, Manenkov AA. 1963. Dynamic polarization of nuclei during saturation of nonuniformly broadened electron paramagnetic resonance lines. *Sov. Phys. Solid State* 5:835–37
- 
- 70. Uses endogenous metal ions as PAs for the investigation of bulk electrode materials.**
- 
- 73. Presents an excellent quantum mechanical treatment of SE and CE theory.**
- 
- 81. Introduces several concepts associated with MAS DNP by paramagnetic metal ions.**
-

83. Borghini M. 1968. Spin-temperature model of nuclear dynamic polarization using free radicals. *Phys. Rev. Lett.* 20:419–21
84. Atsarkin VA, Mefed AE, Rodak MI. 1969. Connection of electron spin–spin interactions with polarization and nuclear spin relaxation in ruby. *Sov. Phys. JETP* 28:877–85
85. Wollan DS. 1976. Dynamic nuclear polarization with an inhomogeneously broadened ESR line. 1. Theory. *Phys. Rev. B* 13:3671–85
86. Wollan DS. 1976. Dynamic nuclear polarization with an inhomogeneously broadened ESR line. 2. Experiment. *Phys. Rev. B* 13:3686–96
87. Hu KN, Yu HH, Swager TM, Griffin RG. 2004. Dynamic nuclear polarization with biradicals. *J. Am. Chem. Soc.* 126:10844–45
88. Song C, Hu K-N, Joo C-G, Swager TM, Griffin RG. 2006. TOTAPOL: a biradical polarizing agent for dynamic nuclear polarization experiments in aqueous media. *J. Am. Chem. Soc.* 128:11385–90
89. Sauvée C, Rosay M, Casano G, Aussenac F, Weber RT, et al. 2013. Highly efficient, water-soluble polarizing agents for dynamic nuclear polarization at high frequency. *Angew. Chem. Int. Ed.* 52:10858–61
90. Matsuki Y, Maly T, Ouari O, Karoui H, Le Moigne F, et al. 2009. Dynamic nuclear polarization with a rigid biradical. *Angew. Chem. Int. Ed.* 48:4996–5000
91. Mathies G, Caporini MA, Michaelis VK, Liu Y, Hu K-N, et al. 2015. Efficient dynamic nuclear polarization at 800 MHz/527 GHz with trityl-nitroxide biradicals. *Angew. Chem. Int. Ed.* 54:11770–74
92. Mentink-Vigier F, Marin-Montesinos I, Jagtap AP, Halbritter T, van Tol J, et al. 2018. Computationally assisted design of polarizing agents for dynamic nuclear polarization enhanced NMR: the AsymPol family. *J. Am. Chem. Soc.* 140:11013–19
93. Kaushik M, Qi M, Godt A, Corzilius B. 2017. Bis-gadolinium complexes for solid effect and cross effect dynamic nuclear polarization. *Angew. Chem. Int. Ed.* 56:4295–99
94. Corzilius B. 2016. Theory of solid effect and cross effect dynamic nuclear polarization with half-integer high-spin metal polarizing agents in rotating solids. *Phys. Chem. Chem. Phys.* 18:27190–204
95. Thurber KR, Tycko R. 2012. Theory for cross effect dynamic nuclear polarization under magic-angle spinning in solid state nuclear magnetic resonance: the importance of level crossings. *J. Chem. Phys.* 137:084508–14
96. Mentink-Vigier F, Akbey Ü, Hovav Y, Vega S, Oschkinat H, Feintuch A. 2012. Fast passage dynamic nuclear polarization on rotating solids. *J. Magn. Reson.* 224:13–21
97. Hovav Y, Shimon D, Kaminker I, Feintuch A, Goldfarb D, Vega S. 2015. Effects of the electron polarization on dynamic nuclear polarization in solids. *Phys. Chem. Chem. Phys.* 17:6053–65
98. Hovav Y, Feintuch A, Vega S. 2013. Theoretical aspects of dynamic nuclear polarization in the solid state—spin temperature and thermal mixing. *Phys. Chem. Chem. Phys.* 15:188–203
99. Ardenkjær-Larsen JH, Fridlund B, Gram A, Hansson G, Hansson L, et al. 2003. Increase in signal-to-noise ratio of > 10,000 times in liquid-state NMR. *PNAS* 100:10158–63
100. Hovav Y, Feintuch A, Vega S. 2012. Theoretical aspects of dynamic nuclear polarization in the solid state—the cross effect. *J. Magn. Reson.* 214:29–41
101. Mance D, Gast P, Huber M, Baldus M, Ivanov KL. 2015. The magnetic field dependence of cross-effect dynamic nuclear polarization under magic angle spinning. *J. Chem. Phys.* 142:234201
102. Hediger S, Lee D, Mentink-Vigier F, De Paëpe G. 2018. MAS-DNP enhancements: hyperpolarization, depolarization, and absolute sensitivity. *eMagRes* 7:105–16
103. Mentink-Vigier F, Vega S, De Paepe G. 2017. Fast and accurate MAS-DNP simulations of large spin ensembles. *Phys. Chem. Chem. Phys.* 19:3506–22
104. Thurber KR, Tycko R. 2014. Perturbation of nuclear spin polarizations in solid state NMR of nitroxide-doped samples by magic-angle spinning without microwaves. *J. Chem. Phys.* 140:184201
105. Mentink-Vigier F, Paul S, Lee D, Feintuch A, Hediger S, et al. 2015. Nuclear depolarization and absolute sensitivity in magic-angle spinning cross effect dynamic nuclear polarization. *Phys. Chem. Chem. Phys.* 17:21824–36
106. Mentink-Vigier F, Mathies G, Liu Y, Barra A-L, Caporini M, et al. 2017. Efficient cross-effect dynamic nuclear polarization without depolarization in high-resolution MAS NMR. *Chem. Sci.* 8:8150–63

---

102. Presents an excellent overview of LACs, depolarization, and practical sensitivity gains under MAS CE.

107. Hovav Y, Feintuch A, Vega S, Goldfarb D. 2014. Dynamic nuclear polarization using frequency modulation at 3.34 T. *J. Magn. Reson.* 238:94–105
108. Bornet A, Milani J, Vuichoud B, Perez Linde AJ, Bodenhausen G, Jannin S. 2014. Microwave frequency modulation to enhance dissolution dynamic nuclear polarization. *Chem. Phys. Lett.* 602:63–67
109. Idehara T, Tatematsu Y, Yamaguchi Y, Khutoryan EM, Kuleshov AN, et al. 2015. The development of 460 GHz gyrotrons for 700 MHz DNP-NMR spectroscopy. *J. Infrared Millim. Terahertz Waves* 36:613–27
110. Yoon D, Soundararajan M, Cuanillon P, Braunmueller F, Alberti S, Ansermet J-P. 2016. Dynamic nuclear polarization by frequency modulation of a tunable gyrotron of 260 GHz. *J. Magn. Reson.* 262:62–67
111. Scott FJ, Saliba EP, Albert BJ, Alaniva N, Sesti EL, et al. 2018. Frequency-agile gyrotron for electron decoupling and pulsed dynamic nuclear polarization. *J. Magn. Reson.* 289:45–54
112. Thurber KR, Yau WM, Tycko R. 2010. Low-temperature dynamic nuclear polarization at 9.4 T with a 30 mW microwave source. *J. Magn. Reson.* 204:303–13
113. Saliba EP, Sesti EL, Scott FJ, Albert BJ, Choi EJ, et al. 2017. Electron decoupling with dynamic nuclear polarization in rotating solids. *J. Am. Chem. Soc.* 139:6310–13
114. Nanni EA, Barnes AB, Matsuki Y, Woskov PP, Corzilius B, et al. 2011. Microwave field distribution in a magic angle spinning dynamic nuclear polarization NMR probe. *J. Magn. Reson.* 210:16–23
115. **Alaniva N, Saliba EP, Sesti EL, Judge PT, Barnes AB. 2019. Electron decoupling with chirped microwave pulses for rapid signal acquisition and electron saturation recovery. *Angew. Chem. Int. Ed.* 58:7259–62**
116. Feintuch A, Shimom D, Hovav Y, Banerjee D, Kaminker I, et al. 2011. A dynamic nuclear polarization spectrometer at 95 GHz/144 MHz with EPR and NMR excitation and detection capabilities. *J. Magn. Reson.* 209:136–41
117. Smith AA, Corzilius B, Bryant JA, DeRocher R, Woskov PP, et al. 2012. A 140 GHz pulsed EPR/212 MHz NMR spectrometer for DNP studies. *J. Magn. Reson.* 223:170–79
118. Leavesley A, Kaminker I, Han S. 2018. Versatile dynamic nuclear polarization hardware with integrated electron paramagnetic resonance capabilities. *eMagRes* 7:133–54
119. Brunner H, Fritsch RH, Hausser KH. 1987. Cross polarization in electron nuclear double resonance by satisfying the Hartmann-Hahn condition. *Z. Naturforsch. A* 42:1456–57
120. Henstra A, Dirksen P, Schmidt J, Wenckebach WT. 1988. Nuclear-spin orientation via electron-spin locking (NOVEL). *J. Magn. Reson.* 77:389–93
121. Hartmann SR, Hahn EL. 1962. Nuclear double resonance in the rotating frame. *Phys. Rev.* 128:2042–53
122. Can TV, Walsh JJ, Swager TM, Griffin RG. 2015. Time domain DNP with the NOVEL sequence. *J. Chem. Phys.* 143:054201
123. Mathies G, Jain S, Reese M, Griffin RG. 2016. Pulsed dynamic nuclear polarization with trityl radicals. *J. Phys. Chem. Lett.* 7:111–16
124. Can TV, Weber RT, Walsh JJ, Swager TM, Griffin RG. 2017. Ramped-amplitude NOVEL. *J. Chem. Phys.* 146:154204
125. Jain SK, Mathies G, Griffin RG. 2017. Off-resonance NOVEL. *J. Chem. Phys.* 147:164201
126. Wind RA, Li L, Lock H, Maciel GE. 1988. Dynamic nuclear polarization in the nuclear rotating frame. *J. Magn. Reson.* 1969 79:577–82
127. Farrar CT, Hall DA, Gerfen GJ, Rosay M, Ardenkjær-Larsen JH, Griffin RG. 2000. High-frequency dynamic nuclear polarization in the nuclear rotating frame. *J. Magn. Reson.* 144:134–41
128. Weis V, Bennati M, Rosay M, Griffin RG. 2000. Solid effect in the electron spin dressed state: a new approach for dynamic nuclear polarization. *J. Chem. Phys.* 113:6795–802
129. Tan KO, Yang C, Weber RT, Mathies G, Griffin RG. 2019. Time-optimized pulsed dynamic nuclear polarization. *Sci. Adv.* 5:eav6909
130. Corzilius B, Michaelis VK, Penzel SA, Ravera E, Smith AA, et al. 2014. Dynamic nuclear polarization of  $^1\text{H}$ ,  $^{13}\text{C}$ , and  $^{59}\text{Co}$  in a tris(ethylenediamine)cobalt(III) crystalline lattice doped with Cr(III). *J. Am. Chem. Soc.* 136:11716–27
131. Ni QZ, Markhasin E, Can TV, Corzilius B, Tan KO, et al. 2017. Peptide and protein dynamics and low-temperature/DNP magic angle spinning NMR. *J. Phys. Chem. B* 121:4997–5006

---

115. Decouples DNP-enhanced nuclear spins close to the electron spin with a frequency-agile gyrotron.

---

132. Daube D, Aladin V, Heiliger J, Wittmann JJ, Barthelmes D, et al. 2016. Heteronuclear cross-relaxation under solid-state dynamic nuclear polarization. *J. Am. Chem. Soc.* 138:16572–75
133. Hoffmann MM, Bothe S, Gutmann T, Hartmann F-F, Reggelin M, Buntkowsky G. 2017. Directly versus indirectly enhanced  $^{13}\text{C}$  in dynamic nuclear polarization magic angle spinning NMR experiments of nonionic surfactant systems. *J. Phys. Chem. C* 121:2418–27
134. Hoffmann MM, Bothe S, Gutmann T, Buntkowsky G. 2017. Unusual local molecular motions in the solid state detected by dynamic nuclear polarization enhanced NMR spectroscopy. *J. Phys. Chem. C* 121:22948–57
135. Aladin V, Vogel M, Binder R, Burghardt I, Suess B, Corzilius B. 2019. Complex formation of the tetracycline-binding aptamer investigated by specific cross-relaxation under DNP. *Angew. Chem. Int. Ed.* 58:4863–68
136. Mao J, Aladin V, Jin X, Leeder AJ, Brown LJ, et al. 2019. Exploring protein structures by DNP-enhanced methyl solid-state NMR spectroscopy. *J. Am. Chem. Soc.* 141:19888–901
137. Aladin V, Corzilius B. 2019. Methyl dynamics in amino acids modulate heteronuclear cross relaxation in the solid state under MAS DNP. *Solid State Nucl. Magn. Reson.* 99:27–35
138. Linden AH, Franks WT, Akbey U, Lange S, van Rossum BJ, Oschkinat H. 2011. Cryogenic temperature effects and resolution upon slow cooling of protein preparations in solid state NMR. *J. Biomol. NMR* 51:283–92
139. Barnes AB, De Paëpe G, van der Wel PCA, Hu KN, Joo CG, et al. 2008. High-field dynamic nuclear polarization for solid and solution biological NMR. *Appl. Magn. Reson.* 34:237–63
140. Zagdoun A, Rossini AJ, Gajan D, Bourdolle A, Ouari O, et al. 2012. Non-aqueous solvents for DNP surface enhanced NMR spectroscopy. *Chem. Commun.* 48:654–56
141. van der Wel PCA, Hu KN, Lewandowski J, Griffin RG. 2006. Dynamic nuclear polarization of amyloidogenic peptide nanocrystals: GNNQQNY, a core segment of the yeast prion protein Sup35p. *J. Am. Chem. Soc.* 128:10840–46
142. Rossini AJ, Zagdoun A, Hegner F, Schwarzwälder M, Gajan D, et al. 2012. Dynamic nuclear polarization NMR spectroscopy of microcrystalline solids. *J. Am. Chem. Soc.* 134:16899–908
143. Lange S, Linden AH, Akbey Ü, Franks WT, Loening NM, et al. 2012. The effect of biradical concentration on the performance of DNP-MAS-NMR. *J. Magn. Reson.* 216:209–12
144. Rossini AJ, Zagdoun A, Lelli M, Gajan D, Rascon F, et al. 2012. One hundred fold overall sensitivity enhancements for silicon-29 NMR spectroscopy of surfaces by dynamic nuclear polarization with CPMG acquisition. *Chem. Sci.* 3:108–15
145. Corzilius B, Andreas LB, Smith AA, Ni QZ, Griffin RG. 2014. Paramagnet-induced signal quenching in MAS-DNP experiments on frozen homogeneous solutions. *J. Magn. Reson.* 240:113–23
146. Andreas LB, Barnes AB, Corzilius B, Chou JJ, Miller EA, et al. 2013. Dynamic nuclear polarization study of inhibitor binding to the M2<sub>18–60</sub> proton transporter from influenza A. *Biochemistry* 52:2774–82
147. Nagaraj M, Franks TW, Saeidpour S, Schubeis T, Oschkinat H, et al. 2016. Surface binding of TOTAPOL assists structural investigations of amyloid fibrils by dynamic nuclear polarization NMR spectroscopy. *ChemBioChem* 17:1308–11
148. Perras FA, Wang L-L, Manzano JS, Chaudhary U, Opembe NN, et al. 2018. Optimal sample formulations for DNP SENS: the importance of radical-surface interactions. *Curr. Opin. Colloid Interface Sci.* 33:9–18
149. Su Y, Andreas L, Griffin RG. 2015. Magic angle spinning NMR of proteins: high-frequency dynamic nuclear polarization and  $^1\text{H}$  detection. *Annu. Rev. Biochem.* 84:465–97
150. Smith AN, Long JR. 2016. Dynamic nuclear polarization as an enabling technology for solid state nuclear magnetic resonance spectroscopy. *Anal. Chem.* 88:122–32
151. Akbey U, Oschkinat H. 2016. Structural biology applications of solid state MAS DNP NMR. *J. Magn. Reson.* 269:213–24
152. Lange S, Franks WT, Rajagopalan N, Döring K, Geiger MA, et al. 2016. Structural analysis of a signal peptide inside the ribosome tunnel by DNP MAS NMR. *Sci. Adv.* 2:e1600379
153. Frederick KK, Michaelis VK, Corzilius B, Ong TC, Jacavone AC, et al. 2015. Sensitivity-enhanced NMR reveals alterations in protein structure by cellular milieu. *Cell* 163:620–28

154. Liao W-C, Ghaffari B, Gordon CP, Xu J, Copéret C. 2018. Dynamic nuclear polarization surface enhanced NMR spectroscopy (DNP SENS): principles, protocols, and practice. *Curr. Opin. Colloid Interface Sci.* 33:63–71
155. Zhao L, Pinon AC, Emsley L, Rossini AJ. 2018. DNP-enhanced solid-state NMR spectroscopy of active pharmaceutical ingredients. *Magn. Reson. Chem.* 56:583–609
156. Lesage A, Lelli M, Gajan D, Caporini MA, Vitzthum V, et al. 2010. Surface enhanced NMR spectroscopy by dynamic nuclear polarization. *J. Am. Chem. Soc.* 132:15459–61
157. Mollica G, Dekhil M, Ziarelli F, Thureau P, Viel S. 2015. Quantitative structural constraints for organic powders at natural isotopic abundance using dynamic nuclear polarization solid-state NMR spectroscopy. *Angew. Chem. Int. Ed.* 54:6028–31
158. Märker K, Pingret M, Mouesca JM, Gasparutto D, Hediger S, De Paëpe G. 2015. A new tool for NMR crystallography: complete  $^{13}\text{C}/^{15}\text{N}$  assignment of organic molecules at natural isotopic abundance using DNP-enhanced solid-state NMR. *J. Am. Chem. Soc.* 137:13796–99
159. Märker K, Paul S, Fernández-de-Alba C, Lee D, Mouesca J-M, et al. 2017. Welcoming natural isotopic abundance in solid-state NMR: probing  $\pi$ -stacking and supramolecular structure of organic nanoassemblies using DNP. *Chem. Sci.* 8:974–87
160. De Paëpe G. 2012. Dipolar recoupling in magic angle spinning solid-state nuclear magnetic resonance. *Annu. Rev. Phys. Chem.* 63:661–84
161. Penzel S, Oss A, Org M-L, Samoson A, Böckmann A, et al. 2019. Spinning faster: protein NMR at MAS frequencies up to 126 kHz. *J. Biomol. NMR* 73:19–29
162. Fernandez-Leiro R, Scheres SHW. 2016. Unravelling biological macromolecules with cryo-electron microscopy. *Nature* 537:339–46
163. Viennet T, Viegas A, Kuepper A, Arens S, Gelev V, et al. 2016. Selective protein hyperpolarization in cell lysates using targeted dynamic nuclear polarization. *Angew. Chem. Int. Ed.* 55:10746–50
164. Rogawski R, Sergeyev IV, Li Y, Ottaviani MF, Cornish V, McDermott AE. 2017. Dynamic nuclear polarization signal enhancement with high-affinity biradical tags. *J. Phys. Chem. B* 121:1169–75
165. Sergeyev IV, Itin B, Rogawski R, Day LA, McDermott AE. 2017. Efficient assignment and NMR analysis of an intact virus using sequential side-chain correlations and DNP sensitization. *PNAS* 114:5171–76
166. Uluca B, Viennet T, Petrović D, Shaykhalishahi H, Weirich F, et al. 2018. DNP-enhanced MAS NMR: a tool to snapshot conformational ensembles of  $\alpha$ -synuclein in different states. *Biophys. J.* 114:1614–23
167. Kubicki DJ, Casano G, Schwarzwald M, Abel S, Sauvee C, et al. 2016. Rational design of dinitroxide biradicals for efficient cross-effect dynamic nuclear polarization. *Chem. Sci.* 7:550–58
168. Geiger M-A, Orwick-Rydmark M, Märker K, Franks WT, Akhmetzyanov D, et al. 2016. Temperature dependence of cross-effect dynamic nuclear polarization in rotating solids: advantages of elevated temperatures. *Phys. Chem. Chem. Phys.* 18:30696–704
169. Geiger MA, Jagtap AP, Kaushik M, Sun H, Stoppler D, et al. 2018. Efficiency of water-soluble nitroxide biradicals for dynamic nuclear polarization in rotating solids at 9.4 T: bcTol-M and cyolyl-TOTAPOL as new polarizing agents. *Chem. Eur. J.* 24:13485–94
170. Soetbeer J, Gast P, Walish JJ, Zhao Y, George C, et al. 2018. Conformation of bis-nitroxide polarizing agents by multi-frequency EPR spectroscopy. *Phys. Chem. Chem. Phys.* 20:25506–17
171. Mentink-Vigier F, Barra A-L, van Tol J, Hediger S, Lee D, De Paëpe G. 2019. De novo prediction of cross-effect efficiency for magic angle spinning dynamic nuclear polarization. *Phys. Chem. Chem. Phys.* 21:2166–76
172. Berruyer P, Emsley L, Lesage A. 2018. DNP in materials science: touching the surface. *eMagRes* 7:93–104
173. Nanni EA, Lewis SM, Shapiro MA, Griffin RG, Temkin RJ. 2013. Photonic-band-gap traveling-wave gyrotron amplifier. *Phys. Rev. Lett.* 111:235101
174. Judge PT, Sesti EL, Saliba EP, Alaniva N, Halbritter T, et al. 2019. Sensitivity analysis of magic angle spinning dynamic nuclear polarization below 6 K. *J. Magn. Reson.* 305:51–57
175. Lee D, Bouleau E, Saint-Bonnet P, Hediger S, De Paëpe G. 2016. Ultra-low temperature MAS-DNP. *J. Magn. Reson.* 264:116–24

---

156. Introduces surface-enhanced NMR spectroscopy by dynamic nuclear polarization (DNP-SENS).

---



---

175. Describes a closed-loop helium MAS for DNP at ultralow temperatures.

---

176. Chen P, Albert BJ, Gao C, Alaniva N, Price LE, et al. 2018. Magic angle spinning spheres. *Sci. Adv.* 4:eaau1540
177. Syed ZH, Kaphan DM, Perras FA, Pruski M, Ferrandon MS, et al. 2019. Electrophilic organoiridium(III) pincer complexes on sulfated zirconia for hydrocarbon activation and functionalization. *J. Am. Chem. Soc.* 141:6325–37
178. Kaur J, Kriebel CN, Eberhardt P, Jakdetchai O, Leeder AJ, et al. 2019. Solid-state NMR analysis of the sodium pump *Krokinobacter* rhodopsin 2 and its H30A mutant. *J. Struct. Biol.* 206:55–65
179. Vowinkel S, Boehm A, Schäfer T, Gutmann T, Ionescu E, Gallei M. 2018. Preceramic core-shell particles for the preparation of hybrid colloidal crystal films by melt-shear organization and conversion into porous ceramics. *Mater. Des.* 160:926–35